Sediment geochemistry and mineralogy from a glacial terrain river system in southwest Iceland

Michael T. Thorpe, Joel A. Hurowitz, Erwin Dehouck

Available online at www.sciencedirect.com

ScienceDirect

Geochimica et Cosmochimica Acta 263 (2019) 140–166

Geochimica et Cosmochimica Acta

www.elsevier.com/locate/gca

Sediment geochemistry and mineralogy from a glacial terrain river system in southwest Iceland

Michael T. Thorpe [a,*], Joel A. Hurowitz [a], Erwin Dehouck [b]

[a] Department of Geosciences, State University of New York at Stony Brook, Stony Brook, NY 11794-2100, USA
[b] Laboratoire de Géologie de Lyon: Terre, Planètes, Environnement, UMR 5276, CNRS, Université Lyon 1, ENS Lyon, Villeurbanne, France

Received 20 June 2018; accepted in revised form 2 August 2019; available online 9 August 2019

Abstract

The weathering of basalt has implications for the global carbon cycle on Earth as well as for understanding sedimentary processes on other terrestrial bodies dominated by a basaltic crust (e.g., Mars), but yet studies in mafic terrains are limited in comparison to their felsic counterpart. Our work details the compositional transformations resulting from the sedimentation process of first-cycle sediments generated in a basalt dominated watershed of southwest Iceland. By sampling multiple sites along the Hvítá S river transport pathway and analyzing the sedimentology, geochemistry, and mineralogy, this work provides a geologically integrated approach to understanding a fluvial source-to-sink system in mafic terrains. Environmental conditions such as climate, hydrology, and transport distance all influence the overall sediment composition, and in response, chemical weathering, physical abrasion, sorting, transport, and mixing are all sedimentary processes unraveled in the geochemical and mineralogical relationships of individual grain size bins. Chemical weathering initiates in the upper reaches of the watershed with the alteration of primary mafic phases to form secondary weathering products. As sediment continues to move downstream, the entire sediment suite becomes more altered, and the extent of chemical weathering is intensified, as evidenced by a higher abundance of clay minerals and glassy material. Fluvial sorting separates detritus by particle size and differentiates them by compositional gradients in geochemistry and mineralogy. As grain size decreases, mafic minerals become less abundant and the finer grain sizes are preferentially enriched in immature weathering minerals and mineraloids (e.g., smectite clays and X-ray amorphous phases). This grain size trend is also correlated with elemental fractionation, illustrated most notably by the clay size fraction (<2 μm) hosting the most altered material in river sediments. However, we note that the environmental conditions of Iceland (e.g., a cold climate and glacial reworking) result in limited element mobility when compared to more temperate climates around the world. Therefore, we suggest that the clay size fraction of river sediments provide a valuable target for understanding the intensity of weathering in these systems, particularly in a colder climate where mineralogical transformations are not always accompanied by a high degree of elemental loss. In addition to weathering and sorting, trace element abundances suggest the mixing of sediments from varying provenances. While the Hvítá S watershed is dominated by basalt, even minor amounts of evolved volcanics (e.g., andesites) contribute to the overall sediment composition. Overall, this work fills a knowledge gap in sedimentation processes in basaltic terrains on Earth, while additionally providing a valuable terrestrial analog for ancient fluvial-deltaic environments preserved in the sedimentary rock record of Mars (e.g., Gale Crater and Jezero Crater).

Keywords: basaltic terrains; river sediments; sedimentation

* Corresponding author at: NASA Johnson Space Center (JSC), USA.
E-mail address: michael.t.thorpe@nasa.gov (M.T. Thorpe).

https://doi.org/10.1016/j.gca.2019.08.003
0016-7037/

1. INTRODUCTION

Chemical weathering and sediment generation in mafic terrains can have a significant impact on geochemical and atmospheric processes at the Earth's surface, however, our understanding of sedimentary processes in such terrains is incomplete. Volcanic rocks only represent a small fraction of the continental surface, with basalt contributing ~3% of the present-day subaerially exposed crust available for weathering (Blatt and Jones, 1975; Meybeck, 1987). However, the weathering of basalt is an important component of the contemporary carbon cycle (Dessert et al., 2003). The nature of source rock lithology has been demonstrated to be one of the main controls on chemical weathering rates and alteration susceptibility, with basalts expressing the highest degree of alteration susceptibility amongst primary silicate rocks (Meybeck, 1986; Bluth and Kump, 1994). This is mainly due to low the temperature alteration of unstable primary Ca- and Mg-bearing silicate minerals and volcanic glass, which are abundant in basaltic rocks, and the weathering of these silicates creates long-term sinks for atmospheric CO_2 (Berner et al., 1983; Berner, 2004). Furthermore, more than 30% of the global atmospheric CO_2 consumed by the weathering of silicates (0.104 GtC/y) is attributed to the weathering of continental volcanic provinces, with ~0.036 Gt of carbon consumed yearly by this process (Gaillardet et al., 1999; Dessert et al., 2003). In light of these contemporary CO_2 consumption rates, the exposure of large-scale basaltic provinces in Earth's history (i.e., continental flood basalts) have been implicated as a driver of global-scale climate change induced by CO_2 consumption during basaltic weathering for the aforementioned reasons (e.g., Berner et al., 1983; Berner, 2004; Rooney et al., 2014). In addition to carbon cycle implications, weathering in basaltic terrains produces chemical and physical denudation rates that exceed global averages (Louvat and Allegre, 1997, 1998; Gaillardet et al., 1999; Dessert et al., 2001; Eiriksdottir et al., 2008; Louvat et al., 2008). Thus, rivers from these environments are transporting a significant flux of sediment and dissolved ions to the oceans, not only impacting the geochemical budget of the ocean but also potentially influencing global climate and biological cycles, e.g., (i) calcium delivery and CO_2 moderation from carbonate precipitation (Gíslason et al., 2006) and (ii) iron cycling and phytoplankton growth (e.g., Raiswell et al., 2006).

Not only is the contemporary weathering of basalts important for the present-day CO_2 cycle and continental fluxes to the oceans, but sedimentary processes in mafic terrains are also significant for understanding critical transitions in the nature of the Earth's continental crust, which is reflected in its sedimentary rock record. Specifically, trace elements in sedimentary rocks deposited at the Archean-Proterozoic boundary record a major change from a mixed mafic-felsic upper crust to a granodioritic upper crust (Taylor and McLennan, 1985; Tang et al., 2016). This Archean-Proterozoic transition is also associated with craton stabilization, thus ancient weathering regimes were altered as a result of more prolific continental runoff (Kump et al., 2000). In turn, the weathering of the continental crust would have stimulated large-scale CO_2 burial and is suggested to coincide with the growth of ancient carbonate platforms (Grotzinger, 1989).

Altogether, it is clear that the weathering of basaltic provinces strongly influence both the modern and ancient Earth geological record but we still lack a full understanding of compositional changes associated with sedimentary processes in basalt dominated terrains. This is largely a consequence of the fact that the bulk of investigations in mafic terrains have concentrated primarily on *in situ* weathering, soil generation, and dissolved and suspended river loads (e.g., Brock, 1943; Bain and Russell, 1980, Nesbitt and Wilson, 1992; Patino et al., 2003; Ma et al., 2007; Babechuk et al., 2014; Eiriksdottir et al., 2008), while the complete history of sediment generation and evolution subsequent to weathering remains unclear. Once entrained in the transportation pathway from *source-to-sink* (Allen, 2008; Grotzinger et al., 2011), the sediment history is largely unaccounted for, presenting a critical missing link in the sedimentation process of mafic terrains. Source-to-sink processes are influenced by a number of intertwined environmental conditions, such as, climate, vegetation, slope, relief, and tectonic setting, all of which are unique to each system (Johnsson, 1993). In response to these factors, chemical weathering, physical abrasion, sorting, transport, and mixing are all variables that impact the overall composition of first-cycle sediment, i.e., sediment derived directly from an igneous source without the influence of crustal-mantle or intracrustal recycling (Taylor and McLennan, 1995). Therefore, the geochemistry and mineralogy of first-cycle sediments can be used to trace the evolution from the pristine protolith in the source terrains to altered detritus in sedimentary deposits, thus tracking the compositional variations imprinted as a result of these sedimentation processes.

The fate of basaltic sediment is the focus of this work, with the aim of contributing a mafic counterpart to well understood sedimentary processes in granodioritic terrains that characterize much of the post-Archean upper continental crust (e.g., Cullers, 1988; Taylor and McLennan, 1985, 1995; Nesbitt and Young, 1984). Our principal goals are to (1) characterize the major, minor, and trace element geochemistry and the mineralogy of basaltic sediments generated in a glacial terrain river system, (2) identify geochemical and mineralogical trends that are associated with various sedimentary processes (i.e., weathering, sorting, transport, and mixing) (3) assess the ability to reconstruct the provenance of mafic sediments transported in a fluvial system from their geochemical properties. Results from our work will provide a better understanding of the physical and chemical processes controlling mafic sediment compositions. This work will also document geochemical and mineralogical transformations that occur as a function of grain size and distance from the source regions. Lastly, our work will place an emphasis on how environmental conditions (i.e., climate, hydrology, and transport distance) play a part in controlling basaltic sediment composition.

2. GEOLOGICAL BACKGROUND, CLIMATE, SAMPLING SITES, SAMPLE COLLECTION AND PROCESSING

2.1. Geological background and study site

Iceland is superimposed on the Mid-Atlantic Ridge (MAR), the location of a divergent plate boundary separating the North American and Eurasian lithosphere plates. At this boundary, the interaction of drifting plates and upwelling magma from a mantle hot spot results in the only subaerial exposed section of the MAR. The surface of Iceland is characterized by a series of ridges, fissure swarms, faults, and volcanoes that closely follow the plate boundary and extend from the southwest to northeast regions of the island (Gudmundsson, 1995).

Altogether, Iceland is dominated by volcanic rocks, covering ~85% of the surface (Sæmundsson, 1979), with the vast majority (>90%) characterized by a tholeiitic composition (e.g., Jakobsson et al., 1978; Sigmarsson et al., 1992; Jakobsson et al., 2008; Thordarson and Höskuldsson, 2008). The study site for this work begins in the central highlands of Iceland at Lake Hvítárvatn, a proglacial lake fed from two outlet channels of meltwater from the Langjökull glacier. Glacial outwash from Langjökull dominates the sediment and fluvial inputs to Lake Hvítárvatn (Larsen et al., 2011). Lake Hvítárvatn is 428 m above sea level and is an open-basin lake that discharges into the Hvítá S River (distinguished herein as *Hvítá S* to denote that we sampled the southern section of the river versus the northwestern branch, which is disconnected from the *Hvítá S* river). The headwaters of the Hvítá S watershed are relatively steep, as illustrated by the stream profile in Supplementary Fig. S1. As the Hvítá S river travels downstream for ~130 km with a northeast to southwest flow pattern, the stream gradient decreases and numerous tributaries join the river. A smaller tributary in the upper reaches of the watershed, the Sandvatn River is sourced from the smaller Langjökull glacier-fed lake and is positioned to the southwest of Lake Hvítárvatn. Eventually, the Hvítá S joins with the Sog River and formally becomes known as the Ölfusá River before discharging into the ocean in the town of Ölfusá (Fig. 1).

Blanketing the mafic rocks of Iceland are Holocene aged volcanic soils, with the majority (~86%) of the soil classified as Andosols (Arnalds, 2004). The soil composition is also influenced heavily by local aeolian inputs, which can vary locally to regionally depending on the relative inputs of large grains (>1 mm) that creep along the surface and fine particulates (<30 μm) that travel in suspension as dust (Arnalds, 2010). These aeolian inputs are sourced from volcaniclastic sandy deserts, located near active volcanoes, and entrained in the dry winds on the leeward side of volcanoes (Arnalds et al., 2016). Generally speaking, young soils in Iceland are mineralogically and geochemically immature owing to the ongoing production of volcanic tephra and redistribution by active eolian processes (Arnalds, 2008). Previous work by Wada et al. (1992) investigated soils in Iceland and determined that they are primarily composed of X-ray amorphous phases, i.e., allophane, imogolite, and ferrihydrite, and generally lacking more mineralogically mature crystalline weathering products such as smectite and kaolinite.

2.2. Current climate regime

During the Younger Dryas (~15–18 ka), glacial cover in Iceland reached its most recent maximum extent. In the Holocene, temperatures began to rise, causing glaciers to retreat (Einarsson, 1984). This warming trend set the stage for the current climate regime, which is classified as subarctic in the Köppen climate classification scheme. Most of the country experiences similar amounts of precipitation throughout all the seasons, and the annual mean temperature is 2.0–5.7 °C, with limited seasonal fluctuation (Einarsson, 1984). Iceland is affected by the mixing of warm air from the upper reaches of the North Atlantic Current with cool artic winds migrating south, which generates significant precipitation in the southwest region of the island. Near the coast, annual precipitation ranges from 1000 to 1600 mm, while inland, the annual range in precipitation totals drop to 700 to 1000 mm (Einarsson, 1984)

2.3. Sample collection, description, and initial processing

In October 2015, we conducted a field campaign and sampled unweathered source rocks, unconsolidated sediment at depositional sites along the Hvítá S River and the accompanying tributaries, and local soil samples, with sampling locations identified on the geological map in Fig. 1 (*see also*, field contextual pictures in Supplemental Fig. S2a–f). Sampling coordinates and sample descriptions are shown in Table 1. A large hand sample, HV004, was selected in the field near the headwaters of the Hvítá S catchment and displayed limited visible signs of chemical weathering (i.e., lack of significant weathering rind or discoloration). Throughout the text, we will refer to this rock as a "reference" source rock for sediments downstream, representing an unweathered basaltic protolith that is broadly representative of Icelandic basalt, as inferred from comparing the total alkali silica (TAS) classification (Supplementary Fig. S3). In addition to igneous sources, soils within the watershed are also likely a source of sediment for fluvial deposits, thus two soil samples (HV002 and HV008) from the surface horizon (A) were acquired to represent the typical soils blanketing the landscape of the Hvítá S catchment. The HV002 soil sample was collected on the plains surrounding Lake Hvítárvatn, while the HV008 soil was acquired in the upper reaches of the Hvítá S watershed on a hillslope above the river.

Sediment deposits were sampled along the riverbanks and bar deposits of the Hvítá S catchment. The unconsolidated sediment was collected using a carbon steel spaded shovel, extracting the top 10–15 cm of material of each sampling target. In this study, we will discuss three depositional sites (SV10A, LG002, and OS001) that extend from the upper reaches of the watershed to the mouth of the river, as shown in Fig. 1 and described in Table 1. The first sampling location, SV10A (also identified in the text as "upstream") was collected closest to the source and

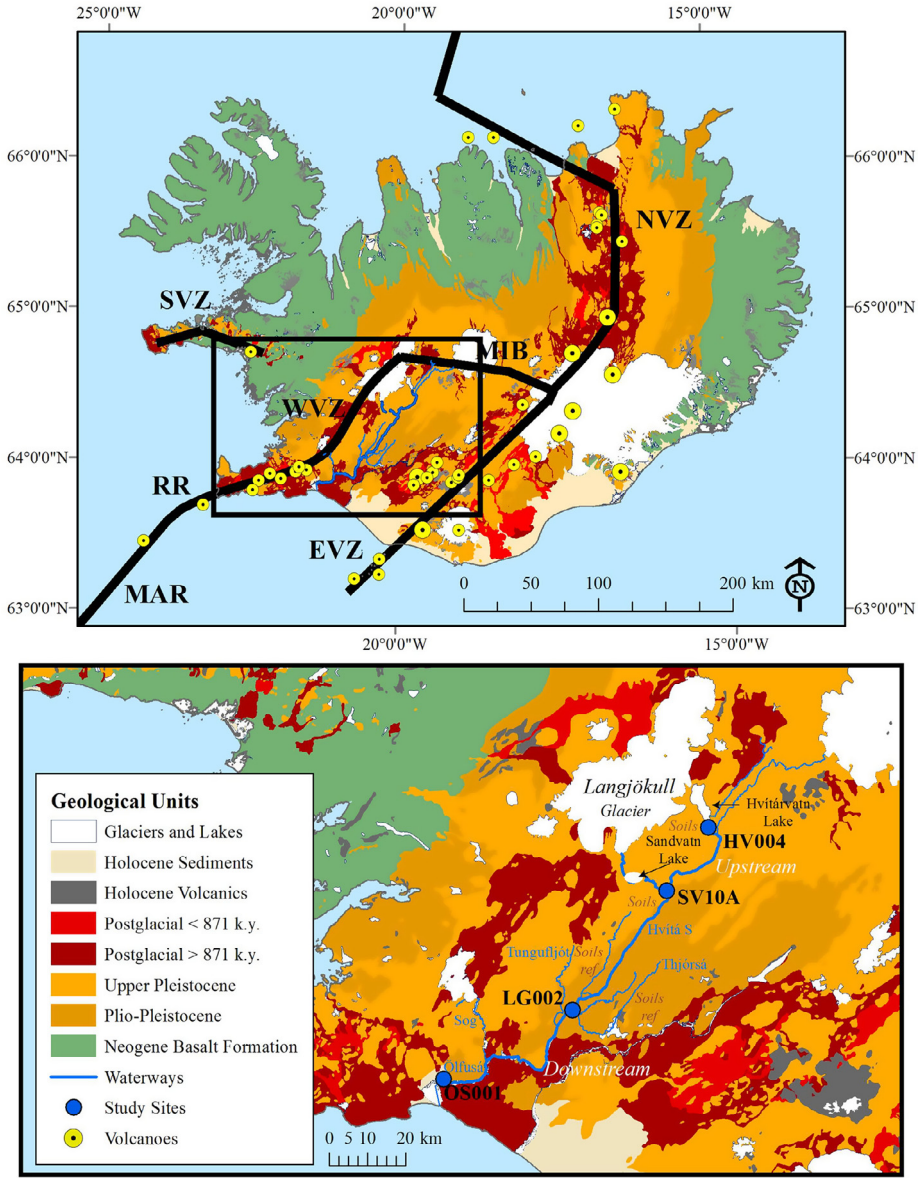

Fig. 1. Geological map of Iceland displaying the ages of basaltic units and with an insert focused on our field sampling locations (blue dots) in southwest Iceland. The geological units are discriminated based on age, with the red to orange color ramp representing basaltic volcanics. In the headwaters of the Hvítá S catchment, the Langjökull glacier feeds meltwater to the Hvítárvatn Lake and represents the source terrains where a hand sample (HV004) was collected as a potential source rock. Sediment samples SV10A, LG002, and OS001 represent the collection locations upstream, downstream, and at the mouth of the river, respectively. Soil samples are displayed and were collected along the transportation pathway of the Hvítá S River. Abbreviations along the Mid-Atlantic Ridge (MAR) are as follows: RR, Reykjanes Ridge; WVZ, West Volcanic Zone; East Volcanic Zone; MIB, Mid-Iceland Belt; EVZ, NVZ, North Volcanic Zone; and SVZ, Snæfellsnes Volcanic Zone. Based on data from National Land Survey of Iceland (https://www.lmi.is/en/stafraen-gogn/) and geological units modified from Johnasson and Semundsson (1989). *Reference soils:* Óskarsson *et al.*, (2012).

~100 m west of the Sandvatan River terminus as it discharges into the Hvítá S, where river deceleration has created a subaerially-exposed river delta. The SV10A deposit consisted of unconsolidated and poorly sorted sediment that displayed layers of darker and coarser (sand to pebble sized) grains to lighter and finer (sand to clay sized) material, as seen in Supplementary Fig. 2a and b as well as Supplementary Fig. 4a, which shows size separates of the sediment after sieving. Sample LG002 (also identified in the text as "downstream") was collected further downstream in the town of Laugarás, where the Hvítá S meets the smaller Tungufljot river and reaches a width of ~175 m. We sampled on the northern bank of the river, from a point bar deposit upstream from where the river bends to the southeast (Supplementary Fig. S2c and d). Qualitatively, the LG002 sample appears better-sorted than

Table 1
A brief description of samples as well as analytical procedures applied to each.

Sample location	Sample ID	Sample description	Coordinates		Elevation (m)[a]	Grain Size (μm)	Mass (g)[b]	Analysis
Source Rock	HV004	Hand sample in the headwaters	64°32′57.85″N	19°47′26.07″W	428	>64,000	–	XRF, QXRD, ICP-MS
Soil Samples	HV002	Soil surrounding glacial lake Hvitarvatn	64°32′35.02″N	19°46′58.03″W	–	–	–	Clay XRD
	HV008	Soil from above upstream River Channel	64°32′0.20″N	19°46′20.06″W	–	–	–	Clay XRD
Upstream	SV10A	Subaerially-exposed river delta. Slightly upstream from the intersection of Sandvatn and Hvítá S Rivers. In the field, a transition from sandy to muddy grains was observed within deposit.	64°23′54.51″N	20° 0′52.55″W	254	>4000	3.6	XRF
						2000–4000	15.6	XRF, QXRD
						500–2000	80.2	XRF, QXRD, ICP-MS
						355–500	19.5	XRF, QXRD
						250–355	11.8	XRF, QXRD
						125–250	22.9	XRF, QXRD, ICP-MS
						90–125	6.7	XRF, QXRD
						63–90	6.9	XRF, QXRD
						45–63	8.8	XRF, QXRD
						<45	6.5	XRF, QXRD, ICP-MS
						<2	–	Clay XRD, ICP-MS
Downstream	LG002	The Laugara depositional site was located downstream from SV10A. The sampling site for this target was a point bar located at a bridge crossing over the Hvítá S river. In the field, this deposit was identified as a sandy/clayey deposit with only a few small pebbles.	64° 6′45.56″N	20°30′40.19″W	58	>500	10.0	XRF, QXRD, ICP-MS
						355–500	10.0	XRF, QXRD
						250–355	30.1	XRF, QXRD
						125–250	34.9	XRF, QXRD, ICP-MS
						90–125	4.0	QXRD
						63–90	4.0	QXRD
						45–63	3.5	QXRD
						<45	9.7	XRF, QXRD, ICP-MS
						<2	-	Clay XRD
River Mouth	OS001	This sample target was named after the Ölfusá river and sampled at the river mouth. This sample mainly consisted of sandy material from sediment on the northern bank of the river mouth.	63°56′27.90″N	21°11′33.94″W	4	>4000	8.9	XRF
						2000–4000	20.7	XRF, QXRD
						500–2000	64.5	XRF, QXRD, ICP-MS
						355–500	24.3	XRF, QXRD
						250–355	21.5	XRF, QXRD
						125–250	39.2	XRF, QXRD, ICP-MS
						90–125	19	XRF, QXRD
						63–90	15.6	XRF, QXRD
						45–63	9.9	XRF, QXRD
						<45	21.3	XRF, QXRD, ICP-MS
						<2	–	Clay XRD, ICP-MS

[a] Elevation above sea level.
[b] Mass of sample after sieved.

SV-10A, and consists of unconsolidated, dark, and poorly sorted sediment (Supplementary Fig. S4b). Lastly, sample OS001 (also identified in the text as "river mouth") was acquired ~7.5 km northwest of the Hvítá S watershed terminus into the ocean (Fig. 1). At this location, we sampled unconsolidated sediment on the northern bank of the river, which reaches a width of ~1 km. At the OS001 site, the river approaches sea level and deposits a significant amount of sediment, creating a delta plain (Supplementary Fig. S2e and f). The OS001 sediment sample is dominated by fine to medium grained sand, with less abundant pebbles (Supplementary Fig. S4c). All samples were stored in plastic containers or cloth bags and shipped back to the Department of Geosciences at Stony Brook University for processing.

Sample processing for the reference rock (HV004) consisted of first cutting the exterior ~1 cm from the hand sample in order to isolate the core of the sample from any potentially weathered material on the exterior. All sediment and soil samples were dried in a low-temperature oven (<60 °C) and then dry-sieved into various grain size fractions with 8–10 bins for each sediment deposit, and with grain sizes ranging from 4 mm to <45 μm, as shown in Table 1. The aim of this grain size processing was to investigate geochemical and mineralogical variability across pebble, sand, silt, and clay grain sizes. Prior to geochemical and mineralogical analysis, the reference source rock sample (HV004) and larger sediment size separates (>250 mm) were crushed with a steel mortar and pestle to particle sizes <250 μm so that they could be fed into a ball mill for further size reduction. All samples were then pulverized in a Retch PM100 Planetary Ball Mill with an agate jar and grinding balls for approximately 10 min at 350 RPM, producing particles <30 μm. Additional sample preparation for each analytical technique is discussed in subsequent sections.

3. ANALYTICAL APPROACH

3.1. GIS and watershed analysis

A geographic information sciences (GIS) watershed analysis was conducted using the Environmental Systems Research Institute, Inc. ArcGIS desktop program called ArcMap and utilized free data from the *National Land Survey of Iceland* (*http://www.lmi.is/en/stafraen-gogn/*) with geological units modified from Johnasson and Semundsson (1989). A 10-m resolution digital elevation model (DEM) of central to southwest Iceland was used to identify the direction of surface water flow, which is then used to predict the magnitude of flow accumulation, a parameter calculated based on the number of raster cells that flow into adjacent cells. The next step was to use this information to identify local areas of high accumulation, ultimately distinguishing a discharge point for rivers and tributaries. Watershed boundaries are then delineated using the points of highest discharge. Once watershed boundaries were identified, we superimposed the surficial geological units and were then able to clip these units to the watershed margins. Performing a raster analysis on the geological unit distribution then provided a useful estimate of the overall abundances of contributing major rock types to sediments deposited along the transportation pathway, from source-to-sink. The area of the catchment was then evaluated by outlining the boundaries with a polygon, as shown in Supplementary Fig. S5. Lastly, a stream profile was generated using *Google Earth*, with the vertical gradient displayed in Supplementary Fig. S1.

3.2. Mineralogy

3.2.1. Quantitative X-ray diffraction

Sample preparation for quantitative X-ray diffraction (QXRD) followed the techniques outlined by Środon et al. (2001) and modified by Eberl (2003). Samples were first wet-ground to fine powders (~5 μm) in a McCrone micronizing mill using zirconium grinding elements with ethanol and a 20 wt% internal standard of Al_2O_3. After low temperature (<60 °C) or air drying, Vertrel XF™, a hydro-fluorocarbon, was added to the sample as a grinding agent and the sample was shaken with three Teflon balls (10 mm diameter) to help produce spherical particles and thus reduce the effect of preferred orientation (Środon et al., 2001). Powders were then front loaded onto a zero-background sample holder and run on a Rigaku MiniFlex600 X-ray diffractometer. XRD patterns were collected using Cu Kα radiation (40 kV, 15 mA) from 5 to 65° 2θ with a D/tex high-speed detector using 0.02° steps and a scan rate of 2° per minute. XRD patterns were analyzed for crystalline phases with the *CRYSTAL IMPACT* software *Match!* using a library of X-ray diffraction patterns from the Crystallography Open Database (COD) to find the best-fit mineral phases for identified peaks. After crystalline phases were identified, mineral abundances were determined by using the *RockJock* XRD pattern fitting program, developed by Eberl (2003), which allows for the quantification of mineral abundances, including poorly crystalline (i.e., poorly ordered) clay mineral and X-ray amorphous phases. Minerals identified from Match! were used as inputs, along with a number of clay minerals, glass phases, and secondary X-ray amorphous materials in the RockJock mineral(-oid) phase library, see also Supplementary Text S1 and Supplementary Table S1.

3.2.2. Clay size fraction mineralogy

For clay mineralogy, the <45 μm fraction that was generated from sieving the bulk sediment was further processed to separate the <2 μm fraction. In brief, ~5 g of the <45 μm sediment was suspended in ultra-pure (18.3 mΩ) water with 0.25 g of potassium phosphate, a salt used to reduce the surface charge on clay minerals, thus limiting clay flocculation, see also Supplementary Text S2. Following Stokes Law, the suspension was then centrifuged to isolate the <2 μm particles and filtered to create an oriented clay peel mount using techniques described in Moore and Reynolds (1997). We measured the clay mount either on the same Rigaku MiniFlex600 diffractometer as the QXRD procedure, with the same operating conditions reported but with scan was ranging from 2.5 to 35° 2θ, or on a Rigaku Ultima, also furnished with a Cu source and a D/tex high-speed detector and operated at 40 kV and 25 mA,

which scanned a two-theta range of 5–35° two-theta. If basal (d_{001}) reflections were identified for swelling clays (i.e., smectites), the sample was subjected to ethylene glycol solvation, which consisted of saturating the sample with ethylene glycol (EG) vapor in a low temperature (60 °C) oven for at least 8 hours. Exposing the oriented clay mount to these conditions will promote the exchange of EG molecules into the interlayer spacing of swelling clays, thus producing a characteristic expansion in these phases (Moore and Reynolds, 1997). X-ray patterns for the EG oriented mount were then acquired on the same instrumentation under the same conditions as the original clay mount. Lastly, the clay size fractions were analyzed in a random orientation and scanned from a two-theta range of 5–65°. This final X-ray analysis of the clay fraction was used to identify any non-clay mineral phases (e.g., pyroxene) and also to distinguish the d_{060} reflections of clay minerals, which can be diagnostic of the clay mineral's octahedral site occupancy, i.e., dioctahedral vs. trioctahedral clay polytypes (Środon et al., 2001).

3.3. Geochemistry

3.3.1. X-ray fluorescence for major and minor elements

For major and minor elements, and selected trace elements, X-ray fluorescence (XRF) spectrometry was employed. Sample preparation followed techniques similar to those described in Norrish and Chappell (1967). Sample powders (<30 μm) were combined with a binding agent, in this case, a cellulose/wax mixture, in a sample to binder ratio of 4:1. The sample/binder mixture was then placed in a centrifuge tube and rotated on an end-over-end sample tube rotisserie for approximately 24 h in order to ensure uniformity in the mixture. Following this, the powdered sample/binder mixture was pressed into pellets using stainless steel and tungsten carbide pressing die and a hydraulic press with 25 tons of pressure exerted on the mixture for five minutes, thus allowing the cellulose to recrystallize. The pressure was then slowly released over an 8-min period in order to prevent decompression cracks from forming, resulting in a 20-mm diameter and 1-cm thick disk.

Pressed pellets were then analyzed on a Bruker S4 Pioneer XRF using the F-Quant mode in the S4 Software package. An 11-point calibration curve was generated with standards from the United States Geological Survey (USGS) that were prepared with the aforementioned sample preparation techniques. Mathematical corrections for absorption effects (Potts, 1992) were performed on the calibration standards. To test the precision of this technique, we ran the USGS Hawaiian Basalt standard (BHVO-2) as an unknown and examined the in-run precision with 5 consecutive measurements and the long-term precision by measuring the sample periodically over the course of six months, with results presented in Supplementary Table 2. The accuracy for this method is compared with certified values complied in Wilson (1998), resulting in an absolute error <2 wt% for major oxides and <36 ppm for trace elements in both the in-run and long-term measurements (*see also* Supplementary Table 2).

3.3.2. Inductively coupled plasma- mass spectrometry for selected trace and rare earth elements

Lower abundance elements required increased instrument sensitivity, therefore selected trace elements and rare earth elements (REE) analysis was performed on an inductively coupled plasma-mass spectrometer (ICP-MS) at the Stony Brook University FIRST Lab on a subset of our sample collection (Table 1). The subset of samples consisted of the reference source rock (HV004), and the >500 μm, 125–250 μm, and <45 μm grain size separates from each depositional site (SV10A, LG002, and OS001). In addition, the clay-size fraction (<2 μm) from SV10A and OS001 were prepared and analyzed with the ICP-MS, however, due to a low sample yield from the clay separation technique in the LG002 sediment, this clay fraction was not analyzed for trace elements. The sample preparation consisted of acid attack using trace element grade hydrofluoric (HF; 48%), hydrochloric (HCl; 38%), and nitric (HNO_3; 70%) acids, following the methodology for sample dissolution described in Potts (1992). The sample was then diluted with 2 vol% nitric to reach a final sample solution of 10 mL and spiked with 100 ppb of indium, used as an internal standard for the ICP-MS measurement, which enables corrections for variations in instrument sensitivity and drift. Powdered USGS rock standards of Hawaiian Basalt (BHVO-2), Icelandic Basalt (BIR-1), and Silver Plume Colorado Granodiorite (GSP-2) were prepared in the same manner and served as an external calibration for measurements of our unknowns. Lastly, BHVO-2a was run as an unknown in order to assess our measurement accuracy, with the absolute error <8 ppm for all trace elements except Cr and Ba, where aboslute error is <21 ppm (*see also* Supplementary Table 3).

3.3.3. Electron microprobe for major elements

The sample mass yield was insufficient for XRF analysis of the major elements in the <2 μm fraction; an electron microprobe analyzer (EMPA) was used instead. EMPA analysis was conducted using a Cameca SX 100 electron microprobe located at the American Museum of Natural History in New York City, NY. Sample preparation for the EMPA consisted of mounting sample powder in a stainless-steel holder (5 mm diameter) in epoxy. The EMPA was operated at 15 kV of accelerating voltage and 20 mA of beam current, with a 5 μm beam diameter spot-size. Measurements were acquired on 9–10 separate spots on each sample and then averaged to yield an approximation of the bulk chemical composition of the clay size separates. We note that the clay fraction is mineralogically heterogeneous, as confirmed from the X-ray diffraction identification of multiple minerals and phases (e.g., quartz, plagioclase, and clay minerals; see results), thus variance in sample composition (Table 2) is likely controlled by sample inhomogeneity over the number of spots analyzed.

Table 2
Major element abundances obtained from EMPA analysis for the clay fraction (<2 μm) of the Hvítá river sediments.

Sample Locality	Upstream		Downstream		River Mouth	
Sample ID	SV10A		LG002		OS001	
	wt (%)	*StDev*	wt (%)	*StDev*	wt (%)	*StDev*
SiO_2	44.94	0.92	42.59	2.17	34.96	2.06
TiO_2	2.48	0.18	3.57	0.27	3.35	0.29
Al_2O_3	24.72	0.71	20.36	0.93	16.63	0.39
FeO_T	11.79	0.66	19.65	1.27	33.68	2.31
MnO	0.22	0.03	0.59	0.07	0.21	0.02
MgO	3.30	0.35	3.25	0.49	2.39	0.13
CaO	8.48	0.39	4.61	0.29	2.94	0.26
Na_2O	1.66	0.10	0.97	0.44	0.62	0.11
K_2O	0.82	0.04	1.10	0.06	1.80	0.12
P_2O_5	1.59	0.14	3.33	0.35	3.42	0.42
CIA	56.48	-	64.60	-	66.68	-
MIA_R	35.91	-	30.11	-	21.14	-
MIA_O	60.22	-	71.35	-	81.75	-

4. RESULTS

4.1. GIS and watershed geology

The Hvítá S is the longest river in southeast Iceland, running for approximately 130 km, with a steep slope in the headwaters (Supplementary Fig. S1.) All local tributaries with a smaller stream order discharge into the Hvítá S, thus creating a 6,688 km^2 area for surface water flow. Our analysis indicates that the majority of the Hvítá S catchment surface area is covered with Pleistocene basalts (Supplementary Fig. S4 and Table S4), with only 18% of the terrain covered in younger, post-glacial basalt. Non-basaltic sources are present in trace abundances. Glaciers and lakes, also situated on basaltic bedrock, compose 14.4% of the surface area.

4.2. Grain size separates

After drying the unconsolidated sediment and soil samples, the mass of each grain size bin was measured (Fig. 2). The degree of sorting can be evaluated graphically with the cumulative frequency patterns (σ_I; *see also* Folk, 1974). All of the Hvítá river sediment deposits are considered poorly to very poorly sorted ($\sigma_I > 1.0$). For the Upstream sediment, SV10A, coarse grained sediments dominated the mass weight fraction, with the 500–2000 μm grain size bin the most abundant. The downstream deposit lacked any sediment with grain sizes >2 mm, while the 125–250 μm grain size fraction was the most abundant and the <45 μm fraction represented 9 wt% of the total mass. Lastly, the 500–2000 μm grain size fraction of the river mouth deposit was most abundant but also contained a large fraction of <45 μm sediment. Although a detailed grain size analysis was not completed on Hvítá S watershed soils, both HV002 and HV008 contain a large fraction of fine-grained material (<45 μm). Furthermore, Icelandic soils investigated in Wada et al., 1992 are composed of approximately 23–73 wt% a clay and silt fraction.

4.3. X-ray diffraction and quantitative abundances

In addition to the following results focusing on the mineralogical abundances returned from RockJock, the X-ray diffraction pattern products are evaluated for low two-theta peaks, diagnostic of clay mineral d_{001} reflections, and evaluated backgrounds, suggesting the presence of an X-ray amorphous scattering phase (Fig. 3; *see also* Supplementary Fig. S6). We note that it is difficult to unambiguously distinguish primary basaltic glass from nanophase or poorly-ordered secondary weathering products (e.g., ferrihydrite and allophane) on the basis of XRD analysis alone (Eggleton, 1987). In 1-dimensional XRD patterns, these two phases lack sharp diagnostic reflections that are characteristic of crystalline phases and instead display broad scattering features (Supplementary Fig. S7). This has implications for our ability to categorize the X-ray amorphous component as primary versus secondary with a high degree of confidence (*see also*, Supplementary Text S3). Despite these complications, RockJock will fit XRD patterns with multiple amorphous components that have the XRD characteristics of volcanic glass and of poorly-crystalline secondary materials that have mixed properties of poorly crystalline (e.g., ferrihydrite) to partially amorphous clay minerals (e.g., smectite + amorphous material. In our samples, components modeled as volcanic glass are very likely a combination of both primary volcanic glass (especially in unweathered source rocks) and secondary amorphous products that have XRD characteristics that are indistinguishable from volcanic glass (especially in river sediments). For accounting purposes, when used in the RockJock pattern fit, we have chosen to separate modeled volcanic glass into a category termed "*glassy material*". On the other hand, phases such as poorly-crystalline weathering products, clay minerals, and hematite are grouped into a category called "*secondary*". Here after, we will speculate on whether the "glassy material" is entirely primary in nature or rather a product of chemical weathering. This discussion will consider the (i) the geological nature of the sample

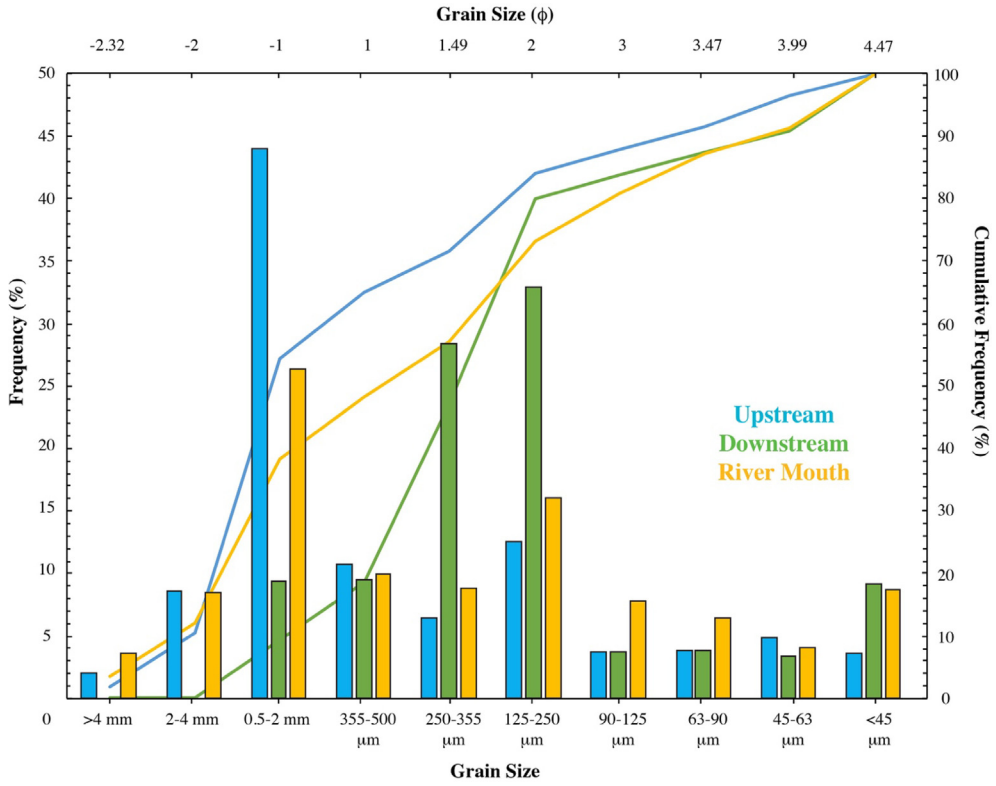

Fig. 2. The weight fraction of grain size bins for each of the Hvítá S river deposits, with both the frequency (bars) and cumulative frequency (lines) plotted.

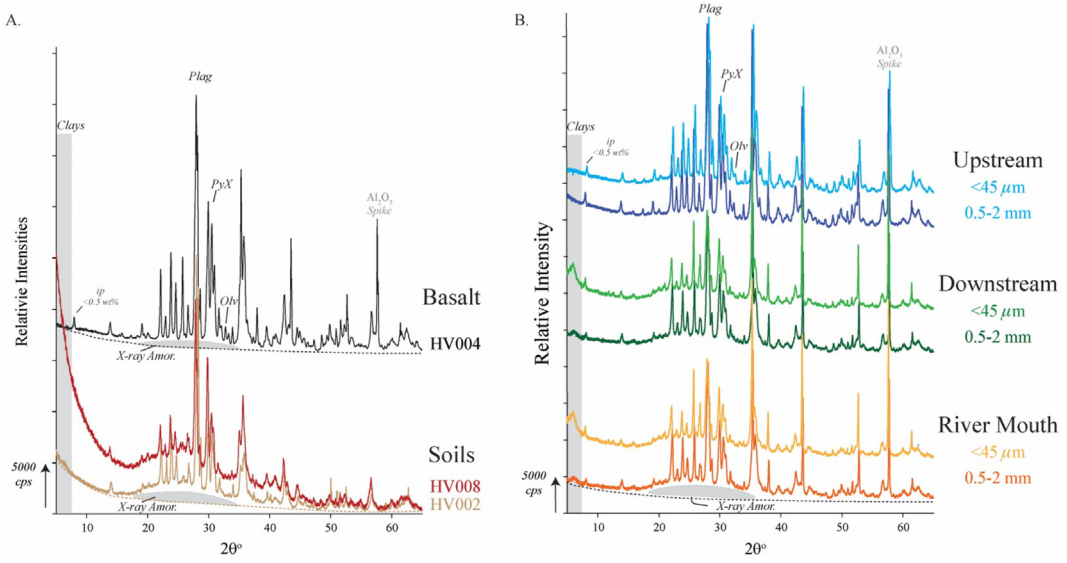

Fig. 3. In panel A, X-ray diffraction (XRD) patterns, offset to identify key features, for the reference basalt, HV004, and two source soil samples, HV002 and HV008. In panel B, XRD patterns for selected grain size bins from the upstream, downstream, and river mouth deposits are displayed. Primary minerals are denoted with the abbreviations Plag: plagioclase; PyX: pyroxene; Olv: olivine; ip: impurity (a contaminate in the Al_2O_3 standard used for QXRD analysis). Clay mineral d_{001} reflections are distinguished by a gray box at low two-theta angles. An inferred instrument background is illustrated by the dotted line. X-ray amorphous (X-ray Amor) material is identified with an elevated background, represented on the figure with a gray "hump". An internal standard of aluminum oxide is labeled Al_2O_3 spike. See text for extended details on trends in the XRD patterns.

(i.e., sediment vs. source rock), (ii) the identification of additional secondary minerals that suggest chemical alteration (e.g., clay minerals), and (iii) the weathering history of the sample as deduced from its chemical composition.

4.3.1. Parent basalt and local soils

The parent basalt (HV004) from the upper reaches of the Hvítá S catchment is dominated by primary mafic minerals, as evidenced by the XRD pattern shown in Fig. 3. Plagioclase and pyroxene are the most abundant primary minerals (51 and 26 wt%, respectively), while olivine is modeled with only a minor abundance (~1.2 wt%). Glassy material and secondary abundances are also modeled to approximately 17 wt%. Given the pristine nature of HV004, the lack of clay mineral d_{001} reflections, and the identification of olivine, we suggest that the sum of glassy material and secondary abundances represents primary basaltic glass with minimal alteration, or at least below the detection limits for the technique used here. Therefore, HV004 represents a reasonable reference rock of unweathered basalt for the purpose of comparison with altered fluvial sediment samples in this study.

For soil samples, HV002 and HV008, mineral abundances are not reported because these samples were not prepared using the QXRD technique; however, mineral phases were identified from examining peak positions in the XRD patterns. As shown on Fig. 3, the XRD patterns for the two soil samples are similar and suggest a comparable mineralogical composition. Overall, both soil samples appear to contain varying amounts of plagioclase and pyroxenes, as inferred from their relative peak intensities. However, the soil samples are also dominated by an X-ray amorphous material (e.g., elevated background from ~20 to 40° 2θ) The reference patterns for ferrihydrite and allophane (Supplementary Fig. S7) display similar scattering features, serving as reasonable candidates for the phases present in the soils, and consistent with the findings of Wada et al. (1992).

4.3.2. Sediment samples

In general, the Hvítá river sediments display an overall increase in glassy material and secondary phases accompanied by a depletion in mafic minerals between the source (HV004) and the river sediments, and between the coarser and finer fractions within and between each sampling location (Figs. 4 and 5). The coarse-to-fine trend is readily observed in XRD patterns of the downstream and river mouth sediments (Fig. 3b, *see also* Supplementary Fig. S6), where the coarse fraction (0.5–2 mm) is dominated by igneous minerals, while the finest fraction (<45 μm) contains clay mineral reflections and an elevated amorphous background. Consistent with these observations, the numerical ratio of mafic minerals/(glassy material + secondary group) decreases from 2.8 (0.5–2 mm) to 1.6 (<45 μm) in the upstream sediment SV10A, from 1.2 to 0.6 in the downstream sediment LG002, and from 0.9 to 0.8 in the river mouth sediment OS001.

For the SV10A sample, we suggest that the "glassy material" in the coarse-grained fraction consists of primary to partially altered basaltic glass, while the intermediate- to fine-grained sediment represents secondary weathering products. This is because, for the SV10A deposit, the XRD patterns for the coarse-grained sediment (>355 μm) closely reflect the HV004 source rock, displaying no evidence for low-angle clay mineral reflections, while the intermediate to fine grain sizes display some evidence for weak clay mineral d_{001} reflections, particularly in the grain sizes bins of 125–250 μm and 45–63 μm (Supplementary Fig. S6). For the downstream and river mouth deposits, clay mineral d_{001} reflections are observed in all of the XRD patterns for size separates, suggesting that the glassy material is partially to completely secondary in nature (Fig. 3, Supplementary Fig. S6). It is also interesting to note that XRD analysis of the coarse grain size fractions of all sediment deposits reveals the presence of secondary minerals (clays, poorly crystalline amorphous phases, etc.), which should have been separated into the finest grain size fractions if they are present as small particulates. Their presence in the coarse fractions suggests either incomplete segregation of grain size fractions, or more likely, that in the coarse sediment, these phases exist as grain replacements, vein and cavity fills, etc., which are not easily removed by mechanical disaggregation and sieving.

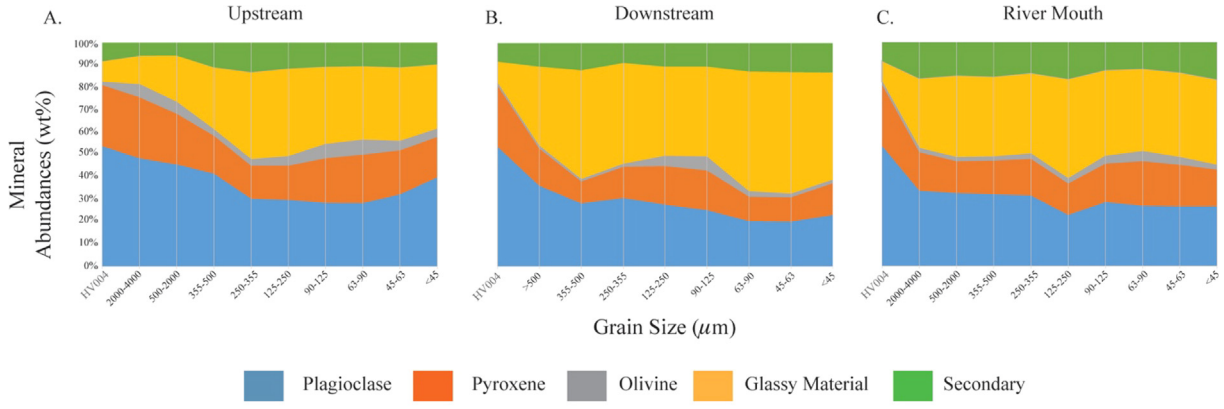

Fig. 4. Mineral group abundances for all three Hvítá river sediment deposits, normalized to 100%, which excludes minor and trace mineral abundances. Grain size bins (gray droplines) decrease from left to right, with the source rock, HV004, used as are a reference pictured furthest to the left. The three panel represent SV10A (a), LG002 (b), and OS001 (c).

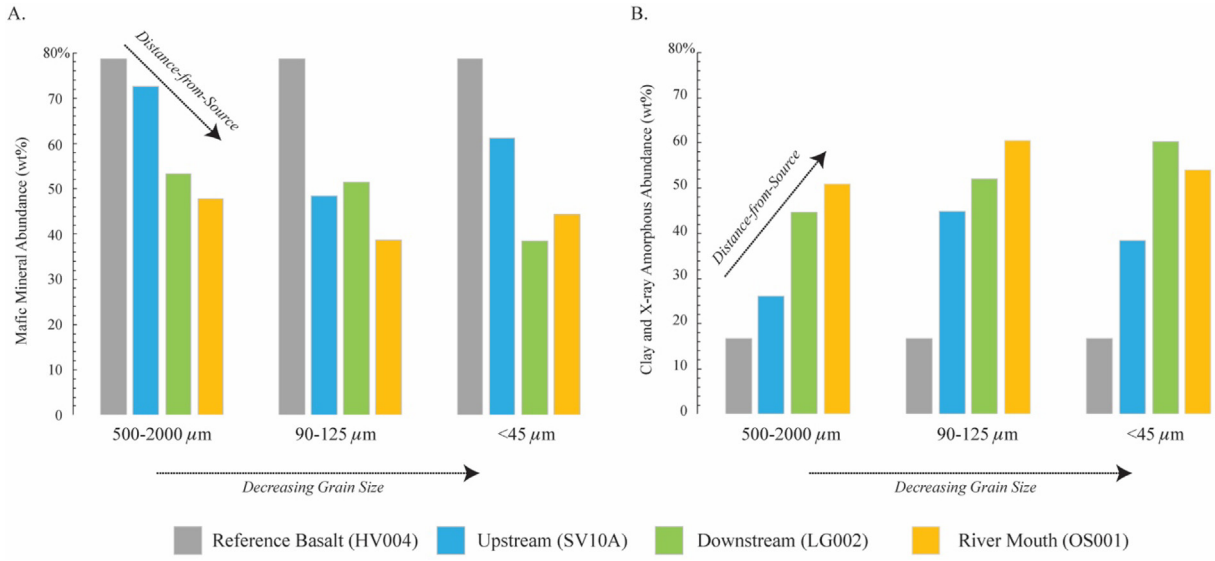

Fig. 5. The sum of mafic mineral (olivine, plagioclase, and pyroxene) abundances (a) and the sum of X-ray amorphous and secondary group abundances (b) for the grain size bins of 500–2000 μm (a), 90–125 μm (b), and <45 μm (c) for all river sediment deposits compared to the reference basalt rock, HV004.

4.4. Clay size fraction XRD

4.4.1. Watershed soils

The HV002 and HV008 clay XRD patterns display no peaks consistent with clay mineral phases (Fig. 6a–b). Instead, both soil samples are composed of an X-ray amorphous phase(s), identified from the elevated background from ~19–34° two-theta, and minor amounts of plagioclase. The two soil samples have varying amounts of X-ray amorphous material (Fig. 6a–b), but overall, display

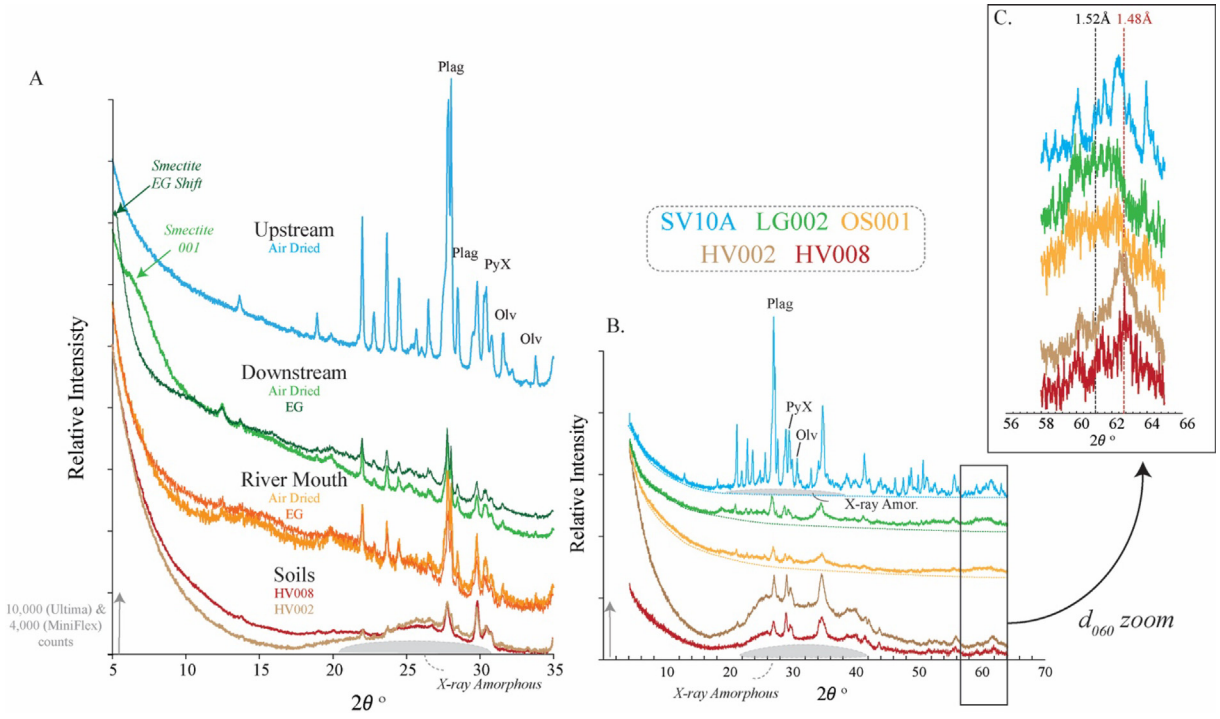

Fig. 6. XRD patterns, offset to identify key features, of the clay size fraction (<2 μm) for the Hvítá river sediments and soil samples, HV002 and HV008. The panels a-c represents XRD patterns for oriented clay mounts both air dried and ethylene glycolated (EG) (a), randomly oriented clay mounts (b), and a zoom of the d_{060} reflection of clay minerals (c). Primary minerals are denoted with the abbreviations Plag: plagioclase; PyX: pyroxene; Olv: olivine. Secondary clays broad reflections and an X-ray amorphous hump is identified.

similar XRD patterns. Lastly, in the randomly oriented powder mounts (Fig. 6c), both soil samples from the Hvítá S watershed display a prominent peak at ~1.48 Å (62.74° 2θ), similar to the XRD patterns of ferrihydrite and imogolite rich Icelandic soils investigated by Wada et al. (1992).

4.4.2. Clay-size sediments

Starting with the upstream deposit, the oriented clay mount for the <2 μm fraction of the SV10A sediment displays that this sample contains a significant amount of primary mafic minerals, i.e., plagioclase and pyroxene, as inferred from the sharp peaks consistent with well-crystalline phases (Fig. 6). Olivine is also identified, but suggested to be less abundant. There are no identifiable reflections for clay mineral phases in the oriented clay mount for the upstream sediments, and therefore, this sample was not subjected to ethylene glycolation. Furthermore, when the randomly oriented powder mounts are investigated for clay mineral phases, only well igneous phases (e.g., plagioclase and pyroxene) are identified in the region where broad d_{060} reflections for clay minerals would be located. However, the absence of d_{001} reflections does not preclude their presence, largely because an overwhelming presence of mafic minerals will hamper the oriented settling of phyllosilicates. Thus, actual clay mineral yield from the sample preparation of a mafic mineral dominated sample may be small. It is also important to note that some of the coarser upstream sediments, from which the clay size fraction is extracted from, display d_{001} reflections for clay minerals (Supplementary Fig. S6). Therefore, while the oriented mount for the upstream deposit does not display strong evidence for clay minerals, they are likely present in a small amount. Furthermore, the randomly oriented powdered diffraction pattern displays a scatter above the background (Fig. 6), consistent with a contribution of X-ray amorphous material. Based on the secondary phases quantified in coarser grain sizes for the upstream deposit, we suggest that this material is at least partially derived from chemical weathering.

In the downstream sediment (LG002), the <2 μm fraction displays a broad d_{001} peak at ~12.6 Å, consistent with a smectite clay mineral, as determined by the shift to 17 Å after being saturated with ethylene glycol (Fig. 6). When the d_{060} reflection is examined, we note broad d_{060} reflection at ~1.52 Å suggesting a dioctahedral smectite. The downstream clay fraction also contains primary mafic minerals (Fig. 6); however, peak intensity is not as strong as in the upstream sediment and thus not as abundant in this sediment deposit, which is also consistent with our analysis of mineral abundances in the downstream <45 μm size fraction (Table 3 and Fig. 5).

The river mouth (OS001) clay size fraction does not display any d_{001} clay mineral reflections (Fig. 6), however, the <45 μm from which this sample was derived from, displays a significant abundance of the secondary phase group (17 wt%), which includes poorly-crystalline clay minerals. In fact, low angle reflections are seen in all other size fractions from this sample (Supplementary Fig. S6). Furthermore, upon investigating the potential d_{060} reflection of OS001, we note a similar peak position between the downstream and river mouth sediment. The river mouth sediment also contains plagioclases and pyroxenes, though not as abundant as in the SV10A sediment (Fig. 6). Lastly, the river mouth clay size fraction displays a significantly elevated background in the XRD pattern, present from ~19 to 34° 2θ, suggesting the presence of an X-ray amorphous phase (Fig. 6).

4.5. Geochemistry

The geochemistry described here represents a combination of: (i) new analyses conducted as part of this contribution using the methods described above and tabulated in Table 4–6 as well as reference values from the literature for (ii) major, minor, and rare earth element (REE) abundances from 30 Icelandic olivine tholeiites (Hemond et al., 1993), (iii) the major, minor, and REE abundances from 3 Icelandic andesites (Hemond et al., 1993), and lastly, (iv) the trace element analysis of 27 basic Icelandic lavas (Wood et al., 1979). All reference values are tabulated in Supplementary Tables S5–S7.

4.5.1. Major element chemical weathering trends

Chemical weathering results from the alteration of pre-existing rocks by meteoric water in sediment source regions, generating sediment/soil horizons enriched in secondary products. In an attempt to quantify the extent of alteration in these profiles, numerous weathering indices have been proposed (Price and Velbel, 2003; and references therein). We use the chemical index of alteration (CIA) (Nesbitt and Young, 1982) as well as the mafic index of alteration (MIA) (Babechuk et al., 2014) to determine the degree to which Hvítá river sediments have been chemically weathered. CIA is calculated as the molar ratio of $[Al_2O_3 / (Al_2O_3 + CaO + K_2O + Na_2O)] * 100$, and similarly, the MIA value (%) is a molar ratio computed from $[(Al_2O_3 + FeO_T) / (Al_2O_3 + FeO_T + CaO + K_2O + Na_2O + MgO)] * 100$. Both these weathering indices document element mobility, which is a consequence of the incongruent dissolution of primary minerals to form secondary weathering products. The major difference between these two weathering indices is the incorporation of elements with mafic mineral affinity, i.e., Fe and Mg, into the MIA calculation, which is of particular interest for basaltic sediments. Both the CIA and MIA juxtapose the behavior of elements (i.e., Al and Fe) that are considered immobile during chemical weathering in low-temperature and well-oxygenated surface conditions, e.g., those pertinent to the fluvial sediments in Iceland, against those that are readily mobilized (i.e., Na, Ca, K, Mg) in the same environments. And while Fe-abundances are reported as FeO_T here, the calculation of MIA treats iron as a weathering conservative element, similar to Al^{3+}, and assumes that Fe^{2+} is efficiently oxidized to Fe^{3+} before any significant leaching occurs. Furthermore, when present as (III) charged species, Al^{3+} and Fe^{3+} reach a solubility minimum in the pH range of natural waters, thus Al- and Fe-bearing phases are expected to be stable during subsequent weathering processes (Stumm and Morgan, 1996; White, 2013). This immobile behavior of Al^{3+} and Fe^{3+} is consistent with the conservation of aluminum

Table 3
Grouped mineralogical abundances obtained from the RockJock pattern fitting software. The detection limit for this technique is generally 1–2 wt%, thus reported abundances below the detection limit should only be considered as the identification of a potential phase.

		Grain Size (μm)	*Degree of Fit*[a]	Plagioclase	Pyroxene	Olivine	Glassy Material	Secondary
Source Rock	HV004	>64,000	0.12	51.3	26.1	1.2	8.9	7.8
Sediments	SV10A	2000–4000	0.12	48.2	27.3	5.7	12.9	5.7
		500_2000	0.10	45.0	22.5	5.0	20.6	5.6
		355_500	0.09	41.1	16.7	2.6	27.7	10.8
		250_355	0.09	29.8	14.4	2.8	38.3	12.8
		125_250	0.08	29.5	14.9	4.1	38.7	11.3
		90_125	0.09	28.2	19.6	6.1	34.3	10.6
		63_90	0.09	27.9	21.3	6.6	32.6	10.2
		45_63	0.09	31.9	19.4	4.1	32.8	10.9
		<45	0.10	39.8	18.0	3.3	29.1	9.4
	LG002	>500	0.09	35.5	16.4	1.4	34.4	10.4
		355–250	0.07	28.0	9.8	1.0	48.0	12.0
		250–355	0.08	30.4	13.7	1.4	44.3	8.8
		125–250	0.09	28.6	18.1	4.7	41.2	10.9
		90–125	0.08	23.2	16.3	5.7	36.8	9.7
		63–90	0.07	20.2	10.8	2.4	52.9	12.6
		45–63	0.07	20.0	10.8	1.6	53.7	12.9
		<45	0.08	22.7	14.1	1.6	47.5	12.9
	OS001	2000–4000	0.08	33.3	16.8	1.5	31.1	15.8
		500_2000	0.08	32.2	14.2	1.5	36.4	14.5
		355_500	0.08	31.8	14.8	1.5	35.6	14.9
		250_355	0.08	31.1	16.2	2.1	35.9	13.3
		125_250	0.07	22.7	13.9	2.0	44.3	16.1
		90_125	0.08	28.3	16.9	3.2	38.1	12.1
		63_90	0.08	26.6	19.4	4.2	36.5	11.6
		45_63	0.08	26.4	18.1	3.3	37.5	13.1
		<45	0.08	26.4	15.9	2.0	37.8	16.2

[a] The degree of fit is the measure of difference between the measured and modeled XRD patterns.

during the breakdown of Al-bearing igneous minerals (i.e., feldspars) into newly formed clay minerals (Goldschmidt, 1937) as well as the limited solubility of ferric-oxides (i.e., hematite) under ambient weathering conditions (Chesworth et al., 1981).

We note the use of *as measured* CaO abundances instead of the typical CaO* values used to correct the CIA value for any calcium present in the non-silicate fraction. The use of non-corrected CIA values is discussed in the supplementary text (S4) however, the net impact is that the reported CIA values represent a minimum, as the use of CaO* will only increase the CIA value. We also note that the clay fraction may inherently have elevated abundances of potassium and phosphate as a product of the sample preparation techniques described in Section 3.2.2, which might have an impact on calculated CIA values. While phosphate in the clay fraction of our Hvítá river sediments is significantly higher than other grain sizes, this may be artificially added to the specimen. Potassium enrichments in the <2 μm sediment are not as apparent, however, the net effect of artificial potassium addition to the clay-size fraction would result in lower CIA values, which can be tested by setting the K_2O abundances in sediment equal to the reference rock (HV004) K_2O abundance. In this modeling exercise, the CIA values for clay-size sediments from SV10A and LG002 experience little change, however, the clay fraction from OS001 is increased from 67 to 70. Therefore, an upper limit on the impact of potassium added to the system from the sample preparation for the clay fraction can be assumed to be ~3 CIA units.

The CIA values for Hvítá river sediments are plotted as a function of grain size and distance from the source in Fig. 7, illustrating relationships between particle size, transport distance, and degree of chemical weathering. All sediments > 90 μm, except for OS001 > 4 mm, plot at low CIA (<45), similar to basalt CIA values. As grain size decreases the CIA values generally increase, with the <2 μm fraction in all sediment samples exhibiting the highest CIA values (>56). The coarsest sediment at the river mouth deposit (>4 mm) has a CIA 46.1, which is somewhat inconsistent with the grain size trend observed from other samples. As the distance from the source increases, the CIA values for the bulk sediment deposit remains relatively unchanged, with the CIA averages ranging from 40.9 to 43.4. In contrast, the <2 μm sediment displays an increase in CIA values as the distance from the source increases. The MIA values are also plotted as a function of grain size and distance from the source in Supplementary Fig. S8. The MIA values span from 40.2 to 81.8 displaying a general correlation with decreasing grain size, though the grain size MIA relationships are somewhat more complex than seen for CIA, potentially stemming from mixed provenance or sorting signatures discussed in further detail in Section 5. On the plot of MIA versus distance from the source, both

Table 4
Major element abundances obtained from XRF analysis for source material and Hvítá river sediments. The chemical index of alteration (CIA) and two forms of the mafic index of alteration (MIA) are also displayed. See text for equations and further explanation.

Sample Location	Sample ID	Grain Size (μm)	SiO_2	TiO_2	Al_2O_3	FeO_T	MnO	MgO	CaO	Na_2O	K_2O	P_2O_5	CIA	MIA_R	MIA_O
Source Rock	HV004	64,000	51.08	2.04	14.42	12.85	0.20	5.54	11.01	2.19	0.40	0.28	37.49	20.39	46.18
Upstream	SV10A	>4000	49.53	1.28	15.52	11.02	0.16	8.59	11.95	1.65	0.20	0.09	38.61	20.01	40.17
		2000–4000	49.59	1.25	15.60	12.27	0.18	6.96	12.06	1.74	0.24	0.11	38.37	20.61	43.62
		500–2000	52.11	1.34	15.50	11.54	0.19	5.76	11.02	1.96	0.44	0.13	39.51	22.09	45.42
		355–500	52.55	1.96	13.69	15.58	0.27	3.67	9.20	2.12	0.73	0.24	39.44	20.71	54.17
		250–355	53.09	2.42	13.24	16.60	0.29	3.41	7.84	1.96	0.91	0.24	41.77	20.73	57.60
		125–250	50.99	3.00	13.64	17.51	0.26	3.56	8.33	1.63	0.80	0.28	42.19	20.61	58.16
		90–125	49.04	3.24	14.40	17.98	0.26	4.29	8.50	1.41	0.59	0.30	43.90	20.82	57.71
		63–90	48.16	3.42	14.06	19.78	0.27	3.52	8.65	1.25	0.59	0.29	43.29	20.25	60.66
		45–63	50.48	2.69	16.75	14.82	0.21	4.27	8.53	1.44	0.49	0.31	47.65	25.00	56.39
		<45	51.72	2.03	17.62	11.81	0.17	5.21	9.12	1.69	0.38	0.25	47.11	26.17	51.06
Downstream	LG002	>500	55.61	2.11	13.04	13.33	0.22	3.91	8.16	2.35	1.02	0.24	39.69	21.14	51.82
		355–500	56.10	2.21	13.16	14.38	0.25	3.24	7.06	2.16	1.16	0.28	42.73	22.15	56.50
		250–355	53.81	2.32	13.33	14.08	0.22	4.47	8.44	2.20	0.86	0.26	40.11	20.66	51.62
		125–250	51.20	2.68	12.32	16.97	0.25	4.86	9.05	1.71	0.70	0.26	38.09	17.92	52.97
		<45	56.56	2.17	13.16	14.05	0.22	4.00	6.88	1.62	1.02	0.32	44.69	22.12	55.64
River Mouth	OS001	>4000	58.05	1.78	13.39	12.79	0.20	4.26	6.08	1.94	1.29	0.22	46.12	23.10	54.41
		2000–4000	55.96	2.07	12.95	14.22	0.21	3.98	7.24	2.12	1.02	0.23	42.17	21.23	54.34
		500–2000	56.15	1.90	13.57	13.27	0.21	3.91	7.39	2.36	1.00	0.23	42.45	22.36	53.38
		355–500	53.42	2.21	13.25	15.39	0.23	4.43	8.12	1.91	0.77	0.26	41.42	20.38	53.97
		250–355	52.69	2.42	13.36	15.95	0.23	4.58	7.87	1.86	0.77	0.27	42.33	20.31	54.73
		125–250	51.55	3.02	12.99	18.09	0.23	3.92	7.57	1.52	0.81	0.28	43.11	19.77	58.82
		90–125	50.50	3.17	13.31	17.75	0.23	4.22	8.28	1.50	0.72	0.33	42.11	19.72	57.06
		63–90	50.55	3.20	13.85	17.49	0.22	4.27	7.96	1.46	0.69	0.31	44.01	20.64	57.64
		45–63	51.05	3.23	14.06	17.07	0.21	4.12	7.81	1.39	0.69	0.35	44.91	21.32	58.04
		<45	52.99	3.10	14.05	17.50	0.21	3.20	6.57	1.26	0.66	0.45	48.82	22.76	63.01

Table 5
Trace element abundances obtained from XRF analysis for source material and Hvítá river sediments.

Sample Location	Sample ID	Grain Size (μm)	Sr	Zr	Cr	Ni	V	Cu	Zn
Source Rock	HV004	64,000	178	145	214	84	398	143	103
Upstream	SV10A	>4000	148	70	344	160	272	128	95
		2000–4000	167	80	339	155	262	123	91
		500–2000	217	182	301	129	243	104	113
		355–500	375	743	162	95	301	93	161
		250–355	313	843	162	97	367	110	187
		125–250	345	495	156	100	455	128	166
		90–125	301	385	203	110	483	154	164
		63–90	322	403	221	139	516	145	167
		45–63	207	262	218	110	446	199	136
		<45	170	171	211	98	369	260	132
Downstream	LG002	>500	267	352	126	58	363	99	146
		355–500	343	484	96	48	341	100	158
		250–355	293	345	133	61	391	109	157
		125–250	281	409	170	110	439	114	161
		<45	185	298	144	53	395	133	143
River Mouth	OS001	>4000	303	403	135	60	286	97	144
		2000–4000	249	331	113	71	360	102	144
		500–2000	271	343	145	66	337	104	144
		355–500	295	388	159	79	389	118	152
		250–355	287	363	167	83	399	125	156
		125–250	348	426	151	95	472	118	175
		90–125	338	379	164	107	494	121	161
		63–90	301	370	189	98	541	132	170
		45–63	286	358	226	104	549	135	177
		<45	230	324	201	86	593	157	157

the weighted MIA averages and <2 μm sediment display an increase in MIA values as sediment is transported further downstream (Supplementary Fig. S8).

A set of ternary diagrams that have seen widespread use in the literature to document chemical weathering trends in weathering profiles are displayed in Fig. 8 (Nesbitt and Young, 1984; Nesbitt and Wilson, 1992; McLennan et al., 1993; Ma et al., 2007; Babechuk et al., 2014). On all ternary diagrams, major elements are plotted in molecular proportions, in order to account for stoichiometric changes during weathering (e.g, Chou and Wollast, 1985; Holdren and Speyer, 1985). The top panels (a,c, and e) in Fig. 8 represent the full extent of the ternary diagrams and also display a weathering trend that is characteristic to *normal basalt weathering* in a soil profile (Nesbitt and Wilson, 1992). The bottom panels (b, d, and f) in Fig. 8 present expanded views of the compositional changes observed in the Hvítá river sediments.

The first ternary diagram we employ is the A-CN-K plot, which places Al_2O_3, ($CaO + Na_2O$), and K_2O at its apices in Fig. 8a. On this triangular plot, volcanic rocks plot at a low Al_2O_3 to ($CaO + Na_2O$) ratio, as illustrated by the position olivine tholeiites and andesites, with the olivine tholeiites plotting closer to the CN apex. All secondary minerals are positioned above this feldspar-join (tie line between plagioclase and K-feldspar), thus chemical weathering on this diagram is represented by a trajectory towards Al_2O_3 enrichment and running subparallel to the A-CN boundary, documenting the breakdown of plagioclase, pyroxene, and volcanic glass and the formation of secondary products (Nesbitt, 2003). The reference source basalt (HV004) plots at a CIA value similar to the average Icelandic olivine tholeiite (CIA = 38 and 37, respectively). The Hvítá river sediments display an overall decreasing grain size trend that runs parallel to the terrestrial basalt weathering trajectory and shows increasing CIA with decreasing particle size (Fig. 8b). Continuing the decreasing grain size trend, the clay-size fraction (<2 μm) for all sediment deposits plot closet to the Al_2O_3 apex. Furthermore, the river mouth sediment (OS001) is most enriched in alumina and represents the most chemically altered sediment on the A-CN-K diagram. These relationships suggest that chemical alteration is a function of both grain size and transport distance (*distance-from-source*), also consistent with the fact that the entire point cloud of the river mouth sediments (OS001) plots further along the weathering array when compared to the upstream deposits.

A common companion plot to the A-CN-ternary, the A-CNK-FM "mafics ternary" diagram (Fig. 8c and d) plots the molecular proportions of Al_2O_3, $CaO + Na_2O + K_2O$, and $FeO_T + MgO$ at its apices (Nesbitt, 2003). This diagram is particularly useful for the analysis for sediments from Iceland because it has the added advantages, in comparison to the A-CN-K diagram, of tracking the behavior of Fe and Mg in olivine, pyroxene, glass, and Fe-Ti oxides. Bulk rock compositions on the A-CNK-FM ternary diagram are positioned based on the proportion of feldspars to mafic minerals, as displayed by the average position of tholeiites and andesites, thus tracking felsic to mafic compositions. Previous work in basaltic weathering profiles

Table 6
Trace element abundances obtained from ICP-MS analysis for source material and Hvítá river sediments.

						Rare Earth Elements (REE)												
Sample Location	Sample ID	Grain Size (μm)	Sc	Th	U	La	Ce	Pr	Nd	Sm	Eu	Gd	Dy	Ho	Er	Tm	Yb	Lu
Source Rock	HV004	64,000	41.80	0.89	0.26	10.76	25.66	3.57	16.79	4.56	1.65	5.07	5.95	1.22	3.41	0.48	2.87	0.41
Upstream	SV10A	>500	32.77	2.34	0.85	9.55	21.76	2.87	12.70	3.28	1.33	3.73	4.23	0.90	2.43	0.36	2.23	0.32
		125–250	28.88	0.91	0.29	38.25	79.97	9.34	39.67	7.98	2.20	7.12	7.09	1.36	3.74	0.52	2.94	0.41
		<45	29.96	1.29	0.49	13.41	30.13	3.99	17.92	4.53	1.51	4.68	5.07	1.03	2.80	0.39	2.36	0.33
		<2	48.48	2.93	0.81	26.22	63.36	7.53	35.47	8.69	2.82	8.37	9.02	1.75	4.85	0.65	3.56	0.49
Downstream	LG002	>500	69.99	5.08	1.69	51.87	113.28	13.64	61.40	14.06	4.13	12.41	13.91	2.64	7.64	1.01	5.32	0.71
		125–250	53.39	3.57	1.24	36.55	72.84	8.31	34.31	6.70	1.73	5.87	5.62	1.11	3.00	0.42	2.50	0.36
		<45	59.26	2.28	0.42	37.55	81.89	9.91	43.50	10.11	2.68	9.19	10.36	2.00	5.70	0.78	4.23	0.58
River Mouth	OS001	>500	37.60	1.33	0.65	35.05	77.50	9.52	42.20	9.69	2.86	8.79	9.72	1.86	5.32	0.72	3.91	0.53
		125–250	42.68	3.63	1.26	33.37	74.08	9.13	40.91	9.36	2.75	8.43	9.01	1.72	4.78	0.64	3.55	0.49
		<45	53.69	3.04	1.22	32.90	74.42	9.36	42.98	10.31	3.05	9.40	10.20	1.96	5.49	0.74	3.97	0.55
		<2	25.89	2.97	1.01	18.15	40.05	5.10	23.62	5.51	1.68	5.41	5.36	1.07	2.89	0.40	2.33	0.33

illustrates that weathering trends cross the feldspar-FM join and trend towards the A-FM join (Nesbitt and Wilson, 1992; Ma et al., 2007; Babechuk et al., 2014). This weathering array suggests the preferential leaching of Ca^{2+}, Na^{+}, Mg^{2+}, and K^{+}, resulting in an Al^{3+} and Fe^{3+} rich residue. The reference source basalt (HV004) is situated near the average olivine tholeiite on the A-CNK-FM ternary. All Hvítá river sediments >2 μm plot in a similar compositional space, appearing as a point cloud between the feldspar-FM join and the reference basalt, consistent with a normal, if not well-developed, basalt weathering trend. When the clay-size fraction river sediments are examined on the A-CNK-FM ternary, we observe that all sediments plot across the feldspar-FM join and display more significant evidence for element mobility. The <2 μm sediments also display a spread in compositional space on the A-CNK-FM ternary, suggesting a diversity in the chemical composition of secondary phases along the Hvítá S River.

Fig. 8f is an AF-CNK-M diagram, which groups the insoluble elements Al^{3+} and Fe^{3+}at the top apex of the diagram, and the soluble elements Ca^{2+}, Na^{+}, K^{+}, and Mg^{2+} along the base of the ternary. On this diagram, the vertical scale represents MIA values, in a manner analogous to the CIA on the A-CN-K diagram (Babechuk et al., 2014) and a general weathering trend runs sub-parallel to the AF-CNK boundary towards the AF apex. When the average composition of volcanic rocks from Iceland are plotted on the AF-CNK-M diagram, the bulk rock composition for olivine tholeiites and andesites are significantly offset from each other (MIA = 37 and 54, respectively), with the tholeiite more enriched in CNK and MgO components relative to the more Al_2O_3-rich andesite composition (Fig. 8). The reference source rock, HV004, lies between the average tholeiite and andesite with an MIA value of 46. When the river sediment samples are plotted on the AF-CNK-M diagram, we first observe that the three coarsest size fractions from the upstream deposit (SV10A) are enriched in MgO compared to the reference basalt. This trend can result from either a sorting of a Mg^{2+} rich phase (e.g., olivine) into the coarser size fraction or the source of sediment for the upstream deposit is more enriched in a Mg^{2+} rich phase compared to HV004. In contrast, the remaining samples plot further away from the MgO apex than HV004, suggesting a preferential mobility of MgO compared to the CNK component. A second trend on this ternary runs sub-parallel to the AF-CNK boundary and towards the AF apex, consistent with continued removal of Ca, Na and K from the samples. The clay-size fraction of all river sediments plots furthest along this second weathering trend. and the river mouth <2 μm sediment (OS001) plots closest to the AF apex relative to the upstream samples, consistent with the previously described grain size and transport distance controlled geochemical relationships.

4.5.2. Provenance tracers (e.g., rare earth element patterns and trace elements)

Rare earth elements (REE) are used to track source rock lithology (i.e., provenance) in sedimentary studies (e.g., McLennan, 1989), largely because they are not easily fractionated during chemical weathering and are transferred

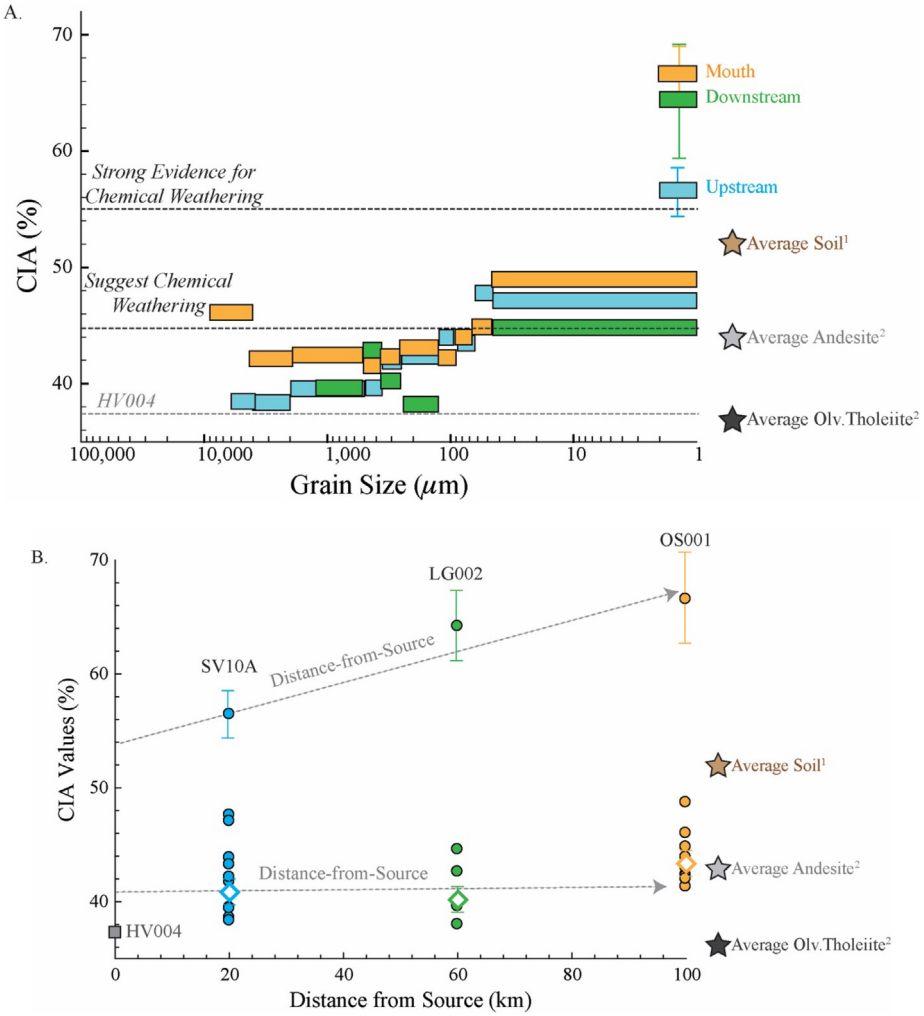

Fig. 7. Grain size bins plotted against CIA values (a) displaying an overall positive correlation, suggesting the most weathered material is separated into finest grain size sediment. In panel b, CIA values are plotted against distance from the source, where little to no change is observed in the CIA weighted averages (diamond open symbol) as distance from the source increases but the <2 μm sediment becomes more altered with increased transport. *References*: [1]*Óskarsson et al.* (2012), [2]Hemond et al. (1993).

quantitatively from source to sediment. The REE patterns of the Hvítá river sediments (Fig. 9) are compared to the reference source rock, HV004, as well as volcanic rock reference patterns from the literature (Hemond et al., 1993) to determine whether sediments in a basalt-dominated catchment preserve the signature of their source(s).

The REE patterns for all Icelandic olivine tholeiites (n = 30) are presented in the bottom panel of Fig. 9 and display a wide range in REE concentrations and patterns that range from relatively flat to patterns that display both positive and negative slopes from light REEs (LREE; La-Sm) to heavy REEs (HREE; Gd-Lu). The average olivine tholeiite displayed in Fig. 9 is characterized by a roughly equal ratio of LREE to HREE. The Icelandic andesite REE pattern shows LREE enrichment, reflecting a more petrologically evolved composition. The source basalt for this study, HV004, is characterized by a slight enrichment of LREE relative to HREE, generating a shallow negative slope in the REE pattern (Fig. 9).

When the Hvítá river sediment REE patterns are compared to the parent basalt and reference volcanic rocks, we observe that the >500 mm grain size fraction from the upstream sediment (SV10A) closely reflects the source rock (HV004) and interestingly, the upstream sediment that is <45 μm also displays a very similar REE pattern. However, in the upstream deposit, the 125–250 μm grain size separate and <2 μm display elevated LREE concentrations and steeper negative slopes toward the HREE (Fig. 9). In comparison, in the downstream deposit (LG002), all sediment samples display an enrichment in the LREE and overall steeper slopes towards the HREE relative to the HV004, with the 125–250 μm grain size bin most concentrated in the LREEs and less concentrated in HREEs. Furthermore, the REE pattern for the >500 mm grain size fraction of the downstream sediment most closely resembles an andesitic pattern. Similar to the downstream sediment, all four grain size bins from the river mouth sediment (OS001) are enriched in the LREE, displaying steep negative slopes,

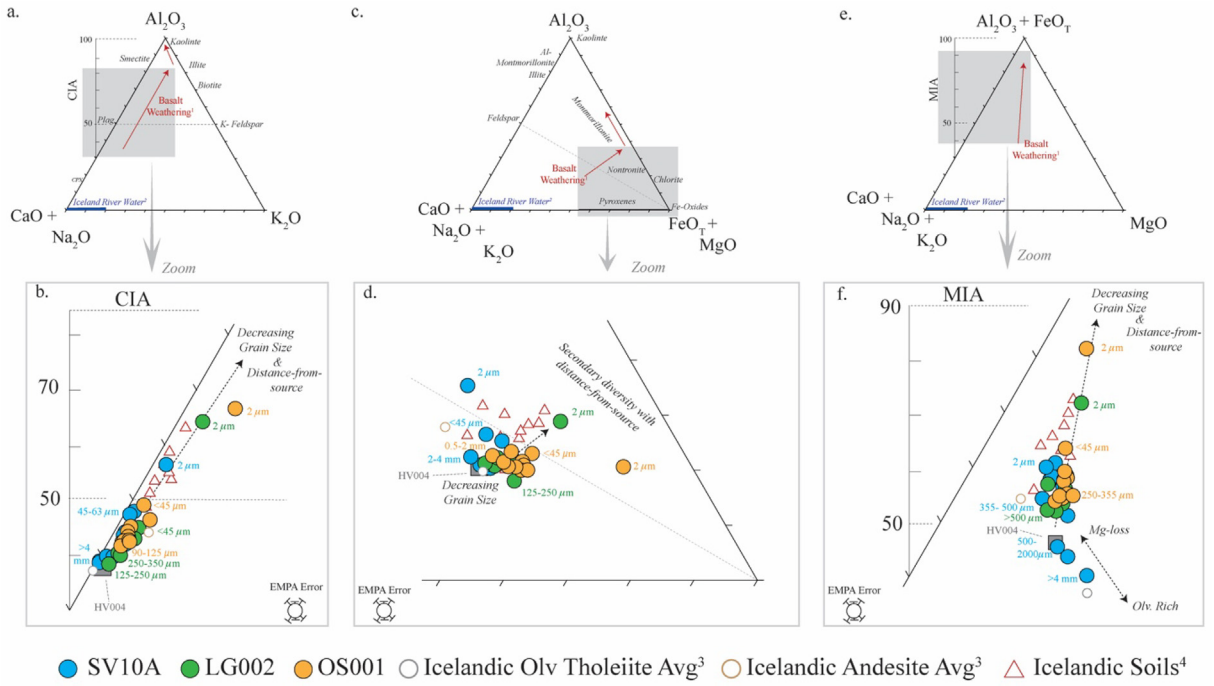

Fig. 8. An overview of terrestrial weathering trends on the A-CN-K, A-CNK-FM, and AF-CNK-M ternary diagrams represented in panels a, c, and e, respectively. A gray shaded box on these ternary diagrams identifies the regions for the zoomed-in views illustrated for each ternary plot in panels b, d, and f, respectively. Error associated with the XRF analysis of the >2 μm sediment is within the symbol size, however, error associated with the EMPA analysis of the <2 μm sediment is displayed. *Reference:* [1]Nesbitt and Wilson (1992).

and only the <2 μm fraction shows a more diluted (i.e., lower ΣREE) pattern.

In addition to the REEs, other trace elements that exhibit variable degrees of mobility can be assessed to track fractionation during sedimentary processes (e.g., sorting and mixing). We compare our data, reported in Tables 5 and 6, to reference values (Supplementary Table S7) for 27 volcanic rocks from Iceland (Wood et al., 1979), which display a transition from mafic volcanic rocks to more slightly evolved volcanic rocks (e.g., basaltic-andesites), as evidenced in the total alkali versus silica diagram (Supplementary Fig. S3). This is an igneous source evolution that has been proposed in numerous Icelandic studies (e.g., Jakobsson, 1972; Sigmarsson and Steinthórsson, 2007). We then establish relationships from these literature and reference values to identify what trace element signatures are retained in sediments of various grain sizes as well as if these signatures are preserved in the sediments transported in the Hvítá S River system.

Scandium, similar to the REEs, is also regarded as a provenance tracer owing to its limited solubility and mobility (McLennan, 1989). Sc commonly substitutes into the crystal structure of mafic minerals (i.e., pyroxene), therefore mafic rocks display Sc enrichment relative to intermediate and felsic sources (Goldschmidt, 1937). The Sc concentration of the Hvítá river sediments ranges from 25.9 ppm (OS001 < 2 μm) to 69.9 ppm (LG002 > 500 μm) with an average concentration of 43.9 ppm. No obvious correlations between scandium concentration and grain size or distance from the source are recognized. In sharp contrast to scandium, thorium and lanthanum are more concentrated in intermediate sources. Icelandic volcanic rocks display a range of incompatible element concentration, with Th ranging from 0.1 to 4.5 ppm, and a La ranging from 0.6 to 47.9 ppm. Our source rock from the headwaters of the Hvítá river (HV004) is unique in regards to incompatible element concentrations, with a Th concentration of 0.9 ppm suggesting a mafic composition but a La concentration of 10.7 ppm more closely resembling a more evolved source. In comparison, the Hvítá river sediments display a range in incompatible element concentrations with the 125–250 μm grain size separate of the upstream sediment representing the least incompatible element enriched sample (Th = 0.9 ppm; La = 9.6), and the >500 μm sediment of the downstream deposit containing the highest concentration of incompatible elements (Th = 5.1 ppm; La = 51.9 ppm). Again, there is no obvious correlation between grain size and incompatible element concentration.

5. DISCUSSION

The river sediments generated and transported in Hvítá S watershed document a complex history that details the effects of chemical and physical weathering, fluvial sorting, and provenance mixing. Unraveling these sedimentary processes by examining compositional changes in the Hvítá river sediments illustrates trends correlated to grain size and transport distance. However, sedimentary signatures preserved in the river sediments are also be impacted by environmental conditions (i.e., climate, hydrology, trans-

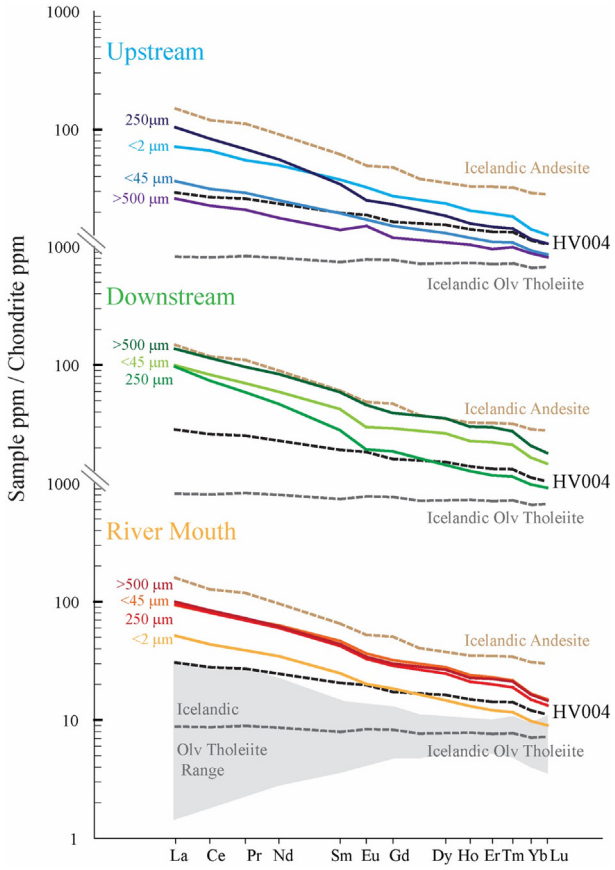

Fig. 9. Chondrite-normalized REE patterns of Hvítá river sediments, a source rock (HV004) from the headwaters of the catchment, a reference envelope for olivine tholeiites, an average from the same olivine tholeiites, and a reference pattern for an andesite from Iceland. Grain size bin 125–250 µm is shortened to 250 µm in the figure text. Reference: Hemond et al. (1993).

port rates, and sediment residence time), thus special care is needed when interpreting the change in sediment composition from the source terrains to depositional sites downstream.

5.1. Weathering

Chemical weathering of the Hvítá river sediments is first documented in the loss of major cations, resulting in element mobility trends that are consistent with an open-system weathering regime (Fig. 8). Chemical weathering is also supported by the observed mineralogical transformations, where the alteration of primary silicate minerals gives way to the increasing abundances of secondary phases (i.e., smectite and X-ray amorphous material). These observed chemical weathering trends in the river sediment composition display first order similarities to the elemental behavior in basaltic weathering profile trends observed in environments around the world (e.g., Nesbitt and Wilson, 1992; Ma et al., 2007; Babechuk et al., 2014). Comparison of chemical weathering trends between fluvial sediments and weathering profiles is equally applicable because the mechanism controlling these chemical weathering trends is ubiquitous, regardless of where the weathering is occurring in the source-to-sink system.

The chemical breakdown of mafic minerals in the Hvítá river sediments is first evidenced on the A-CN-K and A-CNK-FM ternary diagrams, where a weathering array crossing the feldspar join provides strong evidence for the dissolution of plagioclase. In addition to highlighting the overall mafic mineral dissolution, the ternaries used in concert illustrate variability in mineral weathering rates. For example, the two-component weathering array on the AF-CNK-M diagram suggests preferential dissolution of Mg-bearing minerals relative to Ca-, Na-, and K-rich phases (Fig. 8). From this initial weathering trend on the AF-CNK-M diagram, it is reasonable to interpret that the dissolution of olivine and/or pyroxene likely controls the early stages of chemical weathering and element mobility in the Hvítá river sediments, in agreement with the previous studies on the relative susceptibility of basaltic phases to weathering: mafic glass > olivine > pyroxene > plagioclase > Fe-Ti oxides (Goldich, 1938; Craig and Loughnan, 1964; Nesbitt and Wilson, 1992; Gíslason and Arnórsson, 1993; Gíslason et al., 1996).

A correlation between elemental concentrations and mineral abundances reinforces the interpretation of this chemical weathering process and how the dissolution of primary minerals is directly linked to soluble cations being leached from the river sediments (Supplementary Fig. S9). Soluble cations (e.g., Mg^{2+}, Ca^{2+}, and Na^{+}) in the river sediments decreases with grain size and suggests dissolution of mafic phases and element mobility as grain size decrease. Furthermore, the clay size fraction is most depleted in these cations and likely represents a continued leaching of these mobile elements, also consistent with the XRD patterns for these sediments suggest a lower abundance of primary minerals. In contrast, the immobile elements display little to no change with grain sizes >2 µm, however, the clay size sediments document an enrichment in FeO_T and Al_2O_3, likely representing the incorporation of these insoluble elements into the secondary phases.

An important take away message from the elemental composition of the clay size fraction is the overall variability between depositional sites, suggesting mineralogical diversity in the Hvítá river sediments as a function of sample location along the source-to-sink pathway. Moreover, the variability in immobile elements (e.g., alumina and iron) is most pronounced and is likely sourced from compositional differences in the relative abundances of X-ray amorphous and secondary phases in the clay-sized sediment. A useful ternary diagram to identify the contributions from secondary phases, both crystalline and amorphous, plots Si-Al-Fe in compositional space in Fig. 10. On this ternary diagram, we note a distinct separation of the clay-size fraction that results in the <2 µm sediment of the upstream deposit plotting near the coarser sediments and reference basalt, while the <2 µm sediment of the river mouth deposit is situated closer to the iron apex. Furthermore, this ternary plot suggest that the secondary component of the upstream sediments is relatively enriched in a silica rich phase(s), e.g., montmorillonite and/or phase compositionally similar to

the reference basalt, while the downstream and river mouth sediment become progressively enriched in a Fe-bearing phase(s), e.g., ferrihydrite. If we then combine the mineralogy of the clay-size fraction with the chemical weathering trends previously discussed and the FeO_T and silica fractionation observed on this ternary, we can attempt to infer a coherent weathering history of the Hvítá sediments. First, we observe that the <2 μm sediment of the upstream deposit preserves a relatively larger fraction of primary silicates, but yet is also likely enriched in an X-ray amorphous phase(s). Ultimately, this mineralogy of the upstream sediment is supported by its position on the sedimentary ternary plots, as illustrated by its proximity to the coarser river sediments. This implies that the upstream deposit is (i) recording the earlier stages of chemical weathering (i.e., incipient alteration), specifically primary silicates altering to an amorphous and/or clay mineral phase, and (ii) the physical breakdown of primary silicates is also an important process in the upper reaches of the watershed. The second stage in the proposed weathering sequence, is the alteration of pre-existing secondary products, a similar process described by Nahon and Colin (1982) as the phyllosilicate stage. During this stage, the continued loss of mobile cations to solution likely occurs as secondary products evolve to a more clay-rich endmember. The downstream deposit appears to represent this intermediary step, as we observe this deposit is abundant with smectite clay minerals and follows a chemical weathering trend on the sedimentary ternary plots that is consistent with terrestrial trends from basaltic weathering profiles (Nesbitt and Wilson, 1992). The last stage in the proposed weathering sequence is the evolution to Fe-rich amorphous material, consistent with the iron oxi-hydroxide stage from Nahon and Colin (1982). This step involves the enrichment of immobile elements (i.e., Fe^{3+}) into a secondary amorphous product, which we propose is consistent with the mineralogy and geochemistry of the river mouth sediments. This diversity in composition for the clay size fraction of the Hvítá river sediment suggest that chemical alteration continues during transportation and/or altered material is transported further downstream, as a result of fluvial sorting of less dense material (e.g., clay minerals) further downstream.

5.2. Sorting

While the Hvítá river sediment depositional sites are spatially separated, they all display a comparable trend with sediment sorting. Sorting of first cycle sediments is chiefly controlled by the particle size, mineral density, and the overall nature of the depositional environment (Folk, 1974). For this contribution, we define sediment sorting as the process that hydrodynamically separates detritus, ultimately creating a gradient recorded in the sedimentology, geochemistry, and mineralogy of the Hvítá river sediments. This sorting signature is first recorded within the grain size distribution patterns of the Hvítá river sediments (Fig. 2). While, the Hvítá river sediments are considered poorly to very poorly sorted ($\sigma_I > 1.0$), the frequency of sediments within each sieved grain size bin details a segregation of grains along the transport pathway. These patterns

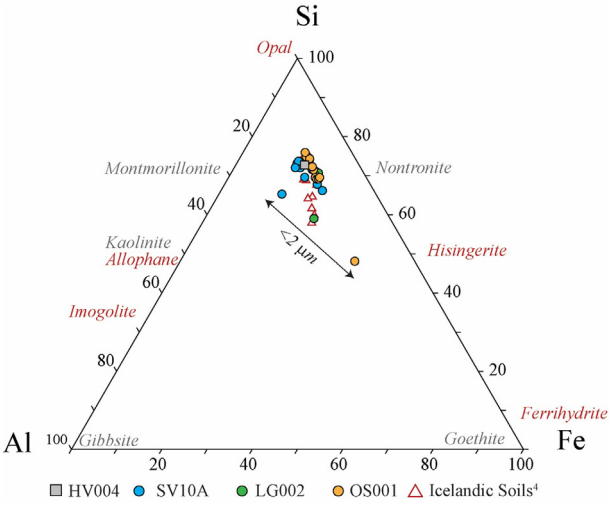

Fig. 10. A Si-Al-Fe ternary diagram demonstrating the silica and iron fractionation in the <2 μm sediment fraction. Secondary crystalline phases (gray text) and amorphous materials (red text) are labeled with compositional spaces reproduced from Eggleton (1987).

in sedimentology alone suggest compositional differences, as previous work by Fedo, McGlynn, and McSween (2015) detailed that parent rocks with multiple modes of phenocryst size can result in a physical separation and redistribution of mineral phases during sorting. This is further supported by the obvious differences in color of grain size bins from the Hvítá river sediments (Supplementary Fig. S4). The extent of physical separation of grains in this study may be biased by the sample collection method in the field (e.g., the ability to access the depositional site) or by the river dynamics (e.g., point bar versus flood plain), however, the overall separation of particles into various grain size bins illustrates a strong control by fluvial sorting.

In addition to the overall sedimentology displaying the net effect of fluvial sorting, grain size separation also creates mineralogical and geochemical trends that are closely associated with chemical weathering. In other words, these processes are difficult to differentiate, largely because they are operating in concert during the sedimentation cycle (Johnsson, 1993; McLennan et al., 1993); however, sorting imprints a grain size signature in both the mineralogy and geochemistry of the Hvítá river sediments. For all depositional sites, the grain size dependency is generalized by the coarse sediment enriched in mafic minerals (i.e. calcic plagioclase, pyroxene, and olivine) relative to the fine-grained sediment, which in turn is chiefly composed of secondary weathering products. As shown on Figs. 4 and 5, a net loss of primary minerals is observed as grain size decreases from the coarsest sediment to the finest particles at each sampling site. For example, in the upstream deposit, the pebble size sediment (>2000 μm) is composed almost entirely of primary minerals (81 wt%), while the <45 μm is made up of 61 wt% primary minerals. Similarly, the river mouth deposit has a drop off in primary mineral abundances from the pebble fraction to the <45 μm sediment (52–44 wt%). As these mineral abundances decline, there

is a net gain in glassy material and secondary phase abundances (Figs. 4 and 5). For instance, the total glassy material and secondary phases more than doubles (19–39 wt%) in the upstream deposit from the pebble to <45 μm fraction. Similarly, the river mouth sediment abundances for glassy material and secondary phases increases from 47 to 54 wt % across the same grain size range.

These mineralogical observations are strengthened with the sorting signature also imprinted on the sediment geochemistry, best illustrated with by CIA values and weathering trends. Previous work by Nesbitt et al. (1996) displayed how sorting impacted sediment composition in sediments derived from granitic to grandioritic provenances, and showed that coarser material was enriched in primary minerals (i.e., quartz) and finer sediment was abundant in secondary products (i.e., clay minerals), thus finer sediment had higher CIA values (Nesbitt et al., 1996). For the Hvítá river sediments, the correlation of sediment grain size and CIA values demonstrates a similar pattern as that described by Nesbitt et al. (1996), where the CIA values increase with decreasing particle size. In fact, the weathering trends on all the ternary diagrams end with the clay size fraction from each river sediment deposit situated furthest along the weathering array. In other words, the clay fraction represents the most chemically altered material relative to any volcanic source material (e.g., the reference source basalt) as well as the coarser sediments. Similar results were detailed in Eiriksdottir et al. (2008), where the clay size fraction of suspended sediments in catchments from northeast Iceland were most enriched in insoluble elements and altered glass. Therefore, by separating the grain sizes of river sediments and analyzing the composition of the finest detritus, we are highlighting the intensity of chemical weathering in the watershed, effectively focusing on the end product of chemical weathering. This finding is critical in the case of the Hvítá river sediments because although there is an overall grain size trend identified with CIA values (Fig. 7), the >2 μm sediments only begin to suggest chemical alteration and it is not until the <2 μm fraction that there is strong evidence for open system weathering. Thus, even with the observed mineralogical transformations in the coarser sediment, the major element geochemistry only changes slightly relative to the reference source basalt for grain sizes >2 μm. In principle, the clay size fraction (<2 μm) should be the repository of the most altered material as this fraction hosts clay minerals and secondary products that naturally form a small crystallite size (Meunier, 2005). However, significant X-ray amorphous and secondary group abundances identified in the coarser sediment suggests that mineralogical transformations in the Hvítá river sediment also occur with only limited element mobility in the coarser sediments.

5.3. Provenance mixing

Ultimately, the Hvítá S catchment samples a significant surface area and even though the watershed is dominated by a progenitor with a basaltic composition, the incorporation of other igneous parent rocks (i.e., mixing) cannot be ruled out. While these non-basaltic provenances only make up a fraction of the exposed geological units in the catchment, these primary sources have the potential to introduce compositional variations in the river sediments. In other words, sedimentary trends, i.e., chemical weathering and hydrodynamic sorting can be misconstrued if the elemental differences and overall weatherability of the parent rocks are not carefully evaluated. Therefore, in this contribution we evaluate mixing, a processes defined as the addition of non-basaltic components (i.e., evolved volcanics) to the overall sediment budget, as another primary component of the sedimentation cycle. Mixing in the Hvítá river sediments may be accomplished by either tributaries carrying a fraction of intermediately sourced detritus and/or pyroclastic material from evolved volcanics distributed along the transport pathway.

The influence of mixing is evaluated by considering two endmember compositions that are proposed for the magmatic evolution of Iceland: (i) olivine tholeiite and (ii) andesite. REE reference patterns for olivine tholeiites and andesites from Iceland (Hemond et al., 1993) display the evolution of volcanic rocks from ultramafic to intermediate compositions. When the REE pattern for the reference basalt from the source terrains of this study is compared to these endmembers, the composition is interpreted to be similar to an olivine tholeiite but slightly more evolved than the reference patterns. The Hvítá river sediments display a wide range in REE concentrations and patterns when compared to the source rock basalt. Some sediments display REE patterns indistinguishable from the source basalt, while others illustrate similar patterns but with an overall increase in total REEs, still others exhibit LREE enrichments. Therefore, even though the Hvítá S watershed is sourced from almost entirely a basaltic lithology, at least one other provenance appears to be contributing to the sediment compositions. First exploring other igneous sources, we investigate the potential contribution of a more evolved volcanic rock composition, i.e., an Icelandic andesite (Hemond et al., 1993). Andesites in Iceland are characteristic of rift zones and display an aerial extent confined to active volcanic areas (Jónasson, 2007). The REE patterns of the Hvítá river sediments suggest that the majority of variability in the REE concentrations can be explained by the mixing of a basalt provenance with an evolved volcanic source (i.e., andesite). However, there does not appear to be an obvious grain size dependency.

Another useful mean of investigating the rock source of the sediments is by comparing trace elements with varying degrees of compatibility. First, an element ratio plot of Th/Sc vs. Zr/Sc compares elements with varying degrees of compatibility and is sensitive to provenance, thus useful in tracking sediments sourced from both mafic and intermediate sources (Fig. 11). While trace element values for scandium from the Icelandic olivine tholeiite and andesite are not recorded in the literature, basic lavas from Wood et al. (1979) demonstrate a spread in trace element ratios governed by a compositional variability in Icelandic source rocks. When the Hvítá river sediments are plotted on this diagram, we observe a scatter away from the reference source basalt, towards more petrologically evolved compositions, however, there is no apparent grain size dependency

for the sediment >2 μm. The clay fraction (<2 μm) from SV10A and OS001 were analyzed for trace elements, and despite the fact that these samples were not analyzed by the XRF technique to obtain zirconium concentration, they are plotted as a line for their respective Th/Sc values. We note that trend of compositional variation observed in the coarser sediment samples continues, with the river mouth <2 μm sediment representing the most geochemically evolved sample. Our interpretation is that this increase in the Th/Sc ratio of the river sediments reflects mixing between mafic detritus and a more evolved volcanic rock source (e.g., Icelandic andesites). Also providing support to this mixing scenario between a more mafic and evolved volcanic rock source, the La-Th-Sc ternary diagram in Fig. 11, displays a distinct separation between the reference basalt rock and river sediment compositions, which can again be explained by the degree of spread in basic lavas from Wood et al. (1979). In this diagram, the <2 μm sediments from SV10A and OS001 again represents the most geochemically evolved sample.

While mixing between different igneous sources is proposed for compositional variability within the river sediments, we also note the potential impact of river sediment mixing with local soils. Although trace element composition of the local soil samples is absent from the literature as well as this study, we assess the influence of mixing soil with river sediment by investigating the major element geochemistry and mineralogy. First, we note that on all sedimentary ternary diagrams and major element plots, the position of local soil reference values (Óskarsson et al., 2012) coincides with the observed chemical weathering trends. However, the major element composition of local soils does not sufficiently detail all the elemental trends with chemical weathering in the river sediments. In other words, the average soil composition is less altered than the clay size fraction of the three Hvítá S river depositional sites. Furthermore, when the mineralogy of the <2 μm particles of the river sediments and soil samples is compared, we note differences in the relative proportions of X-ray amorphous material, but more importantly, the identification of dioctahedral smectites is absent from the soil samples. Thus, while it is likely that local soil is mixed with the river sediment along the sediment transport pathway in the Hvítá S, it does not sufficiently explain all the chemical weathering trends observed in the fine-grained sediment composition.

5.4. Influence of environmental conditions (climate, hydrology, and transport)

The Hvítá S watershed samples a significant portion of southwest Iceland and this work provides constraints on chemical and physical weathering trends manifested during sedimentation in basaltic terrains. However, we also recognize that there are environmental conditions that may impact our sediment sample compositions in ways that we have not considered as a part of this work. Thus, in this section we highlight some additional factors that need to be considered in future work aimed at evaluating sediment composition and how they might influence the way we interpret sedimentary processes in basaltic terrains.

5.4.1. Climate

When compared to basaltic weathering profiles in temperate climates (e.g., Nesbitt and Wilson, 1992; Ma et al., 2007; Babechuk et al., 2014), the Hvítá river sediments never reach an advanced chemical weathering stage (i.e., CIA > 85). While there are additional environmental factors that may influence the alteration state of the river sediments, as detailed below in Section 5.4.2, here we describe the impact of climate on the weathering intensity of the Hvítá S river sediments. Specifically, we will focus on how the colder temperatures in southwest Iceland play a role in the overall reaction kinetics of weathering basalt.

Temperature has a significant impact on the weathering rates of silicate minerals (Lasaga et al., 1994; White et al., 1999; Kump et al., 2000; Brantley, 2003), thus, warmer climates are characterized by higher weathering rates and increased weathering fluxes of dissolved species (White and Blum, 1995; White and Brantley, 1995; Gaillardet et al., 1999; Dessert et al., 2003). Placing the climate of southwest Iceland, which ranges from 2.0° to 5.7 °C, in context with tropical and temperate climates from around the world (Gaillardet et al., 1999), it is expected that the chemical weathering rates should be significantly lower in the Hvítá S catchment. Previous work by Louvat et al. (2008) supported this notion by comparing cold river waters of Iceland to warmer river waters from Réunion, Sao Miguel in Azores, and Java, finding that Iceland had lower chemical denudation rates and suggested this was a product of the frigid temperatures. Therefore, slower reaction kinetics in a cold climate need to be considered as a possible factor contributing to the lower CIA values observed in the Hvítá S river sediments. However, it is also interesting to note that although CIA values are relatively low, X-ray amorphous and secondary phases make up a significant fraction of the mineralogy for the downstream and river mouth sediments. Thus, in a cold climate, chemical weathering indices may be relatively insensitive due to limited element mobility, while mineralogy will reveal a complex suite of immature weathering minerals and mineraloids that reflect the incomplete nature of weathering processes in cold climates.

5.4.2. Hydrology, transport distance, and residence time

The Hvítá S catchment is first sourced from the Langjökull glacial melt waters feeding the Lake Hvítárvatn, where the turquoise hue of the lake water is indicative of a significant load of suspended sediments (e.g., glacial flour). In the upper reaches of the watershed, the Hvítá S river migrates across a steep gradient until it approaches a knickpoint at the Gullfoss waterfall (Supplementary Fig. S1). The river slope then levels off and gradually descends downstream in the lowlands of southwest Iceland. Before discharging into the Atlantic, numerous tributaries join the Hvítá S river, some of which are sourced from a non-glacial fluvial system.

We emphasize the hydrology of the Hvítá S watershed because it can have a significant impact on the overall sediment compositions, particularly because Icelandic watersheds have been previously noted for having high rates of mechanical erosion, e.g., Gíslason et al., 1996; Louvat et al., 2008). For example, in the upper reaches of the water-

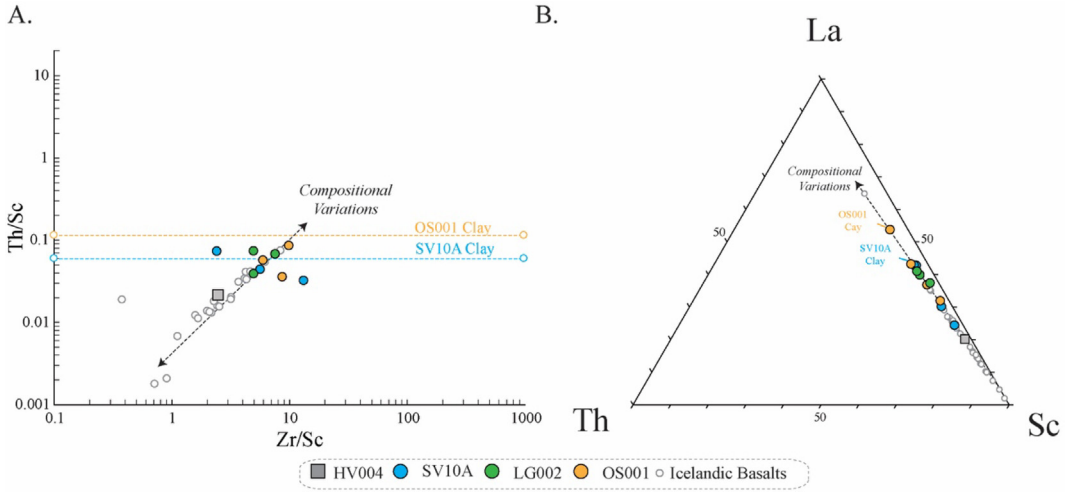

Fig. 11. A plot of Th/Sc vs. Zr/Sc (a) identifies trace element compositional variations for the Hvítá river sediments, with reference materials for basic lava from Iceland also plotted. The clay fraction from SV10A and OS001 were analyzed for the trace elements Th and Sc, with this ratio plotted extending the entire Zr/Sc range. The LG002 clay fraction was not analyzed. A companion ternary plot of La-Th-Sc (b) compares elements of varying degrees of compatibility and illustrates a spread in river sediments trace element composition, potentially consistent with the input from variable provenances. Error is contained within the symbol size. *Reference for Icelandic Basalts:* Wood et al. (1979).

shed, the influence of glacial flour production and a high sediment flux due to a steep gradient may create a scenario where physical weathering surpasses chemical weathering. Furthermore, this could also lead to the variation with grain size distributions observed in the various Hvítá S depositional sites (Fig. 2). Evidence for physical transport playing a large role in the dynamics of Icelandic river chemistry is documented in Gíslason et al. (2006), where the authors determined that suspended sediment flux was chiefly controlled by discharge rates, i.e., higher discharge rates resulted in rivers carrying more sediment. A similar mechanism was detailed in Eiriksdottir et al. (2008), where high mechanical erosion rates in catchments from the northeast of Iceland led the authors to propose that almost completely unaltered sediment was being delivered to the oceans. However, when we calculate the CIA values of the suspended sediments investigated in Eiriksdottir et al. (2008), an average CIA value of 62 is directly in line with the clay fraction of the upstream river sediments (CIA = 60.2) in the present study, thus, we would consider these CIA values to suggest chemical weathering. Regardless, while the relatively low CIA (<65) values are likely linked to a colder climate, increased physical weathering and a high sediment flux are factors that also need to be considered as a likely source for the combined delivery of unweathered and slightly altered detritus downstream.

Another important hydrologic consideration is the catchment source, i.e., glacial versus non-glacial watersheds can produce sediments with variable compositions. Previous work by Gíslason et al. (1996) demonstrated that the dissolved load in Icelandic river waters is strongly influenced by the glacial cover within the catchment. Additional work by Hawley et al. (2017) demonstrated that non-glacial watersheds resulted in a higher degree of chemical weathering while glacial sourced rivers were characterized by a higher degree of sediment flux. When this is put into the context of the Hvítá S depositional sites for this study, we note that the upstream deposit is entirely sourced from a glacial catchment where physical erosion may be more important than chemical weathering. On the other hand, the downstream and river mouth depositional sites have a larger tributary network that may source inputs from non-glacial sediment, potentially allowing for a higher degree of alteration in these samples.

In addition to the local hydrology and river inputs, another means of altering the Hvítá S sediment composition is through the transport and storage mechanisms of sediment from source-to-sink, variables that are poorly constrained in the literature for mafic sediments. Such an example of a transport process that can impart compositional changes on sediment is the buildup of detritus at temporary storage sites (e.g., floodplains) along the sediment transportation pathway. As sediment accumulates at these sites, the sediment is exposed to surficial weathering conditions, similar to those exhibited by a weathering profile in the source terrains. Previous work by Bouchez et al. (2012) demonstrated that sediments transferred into the floodplains of the Amazon River displayed signs of elemental lost consistent with the continued dissolution of primary minerals. While it is difficult to say if this is case for the Hvítá S river sediments, the continued alteration of sediment during transport and temporary storage may in part be reasonable for the diversity of mineral phases in the clay fraction from the three spatially separated depositional sites in this work. A conceivable alteration scenario would entail the weathering of unaltered detritus to form new secondary products and/or the continued alteration of pre-existing secondary products stored with the sediments to form new phases, e.g., neoformed clay minerals (Merriman, 2005).

6. CONCLUSIONS

The composition of sediment generated in the Hvítá S watershed of southwest Iceland documents a history of chemical weathering, fluvial sorting, and sediment mixing that continues along the transportation pathway from source-to-sink. The geochemical and mineralogical analysis of sediment from three different depositional sites along this glacial river records signatures of these sedimentary processes, all of which are likely impacted by a number of environmental conditions. This contribution unravels these sedimentary trends and environmental signatures, thus furthering our understanding of sedimentary processes in basaltic terrains and also provides a missing link in the sedimentary cycle from which the compositional transformation from source-to-sink are largely overlooked.

Chemical weathering is the principal control on the composition of Hvítá river sediment, responsible for major element mobility and primary silicate mineral and mafic glass breakdown. The chemical weathering trends observed in southwest Iceland display first order similarities to those observed in basaltic weathering profiles from around the world (e.g., Nesbitt and Wilson, 1992; Ma et al., 2007; Babechuk et al., 2014). These weathering arrays are produced when basaltic minerals are exposed to subaerial weathering conditions resulting in the leaching of Mg^{2+}, Ca^{2+}, and Na^{+} into solution. While there is a preferential dissolution of Mg-bearing phases (e.g., olivine and pyroxene), the net effect on mineralogy is a decrease in primary igneous minerals and an increase in secondary weathering products.

In addition to chemical weathering, sediment sorting during fluvial transport results in a separation of detritus at each depositional site within the Hvítá S catchment based on grain size and mineral density. A detailed analysis of individual grain size bins reveals a compositional gradient in both geochemistry and mineralogy as grain size decreases. This sorting trend results in the coarse sediment enriched in Mg^{2+}, Ca^{2+}, and Na^{+} relative to a fine-grained fraction with a higher abundance of immobile elements, i.e., iron and alumina. Furthermore, mineralogical analysis details a coarse fraction with significant mafic mineral (i.e., pyroxene, plagioclase, and olivine) abundances compared to the fine grained sediment enriched in clay minerals and amorphous phases material.

While the Hvítá river sediment composition is largely controlled by chemical weathering and sorting, the trace element geochemistry of these sediments also demonstrates the impact of mixing sediment from various igneous sources. The REE patterns of grain size separates suggests that even minor amounts of evolved volcanic rocks can alter the sediment composition, thus adding complexity to tracing the provenance from source-to-sink in a fluvial system. The Hvítá S watershed is dominated by basalt, however, volcanic zones in Iceland produce andesitic to rhyolitic rocks and tephras, consequently providing a source of evolved sediment to enter the system. Although the volumetric significance of these Holocene evolved volcanics is small, the trace element geochemistry documents the mixing of an intermediate source, e.g., an andesitic composition. Thus, this work demonstrates that the even in a basalt-dominated watershed, mixing of basalt with minor inputs from an intermediary source likely plays a key role in trace element composition of river sediments. In addition to mixing igneous sources, adding local soil to the fluvial sediment is also a potential source of compositional variability, likely impacting the overall mineralogy the finest detritus.

The sedimentary processes described above are almost certainly impacted by the environmental conditions (climate, hydrology, and transport) of the Hvítá S catchment. These environmental conditions can imprint a signature that either enhances or hampers the influence of chemical weathering, sediment sorting, or provenance mixing. For example, the fluvial gradient (e.g., river slope) and river source (non-glacial versus glacial) may increase the total flux of unweathered detritus and result in the upstream deposits to be less altered. However, sediment residence time at temporary storage sites (e.g., flood plains) along the transportation pathway exposes detritus to surficial weathering conditions and can further alter the sediment. Thus, it is critically important to understand the hydrology and nature of the system when interpreting the overprint of sedimentary processes on the sediment composition.

The analysis of sediments from a basalt-dominated watershed demonstrates the importance in tracking sediment composition from source-to-sink. In general, chemical weathering has largely been regarded as a process that occurs in the source regions, mobilizing elements during pedogenesis, and with all subsequent chemical alteration only occurring syn- to post- deposition, thus the sediment compositions at local fluvial depositional sites is largely overshadowed. Between chemical weathering and physical sorting, the fine-grained sediment in fluvial deposits exemplifies the degree of alteration in the system and provides a useful target to develop a complete story of sedimentary processes in a particular system. Here, we have demonstrated that compositional changes in fluvial sediments are significant between upstream and downstream deposits, documenting an increase in chemical weathering indices and secondary phases with an increased distance from the source. These variations in composition are likely a combination of environmental conditions and sedimentary processes, both of which need to be considered when evaluating the sediment transformations from source-to-sink. Lastly, the results of this work also have planetary implications, as regions of Mars, e.g., Gale Crater and Jezero Crater preserve a rich sedimentary history of fluvial processes in basaltic terrains (Grotzinger et al., 2011; Hurowitz et al., 2017; Rampe et al., 2017; Goudge et al., 2018). Thus, environments like those investigated in this study may serve as valuable martian analogs and aid in developing a better understanding of sedimentary processes on planetary bodies.

ACKNOWLEDGEMENTS

This work was supported by a NASA Earth and Space Science Fellowship (award #NNX15AT58H to M.T.T.), the NASA Solar System Workings program (award #NNX16AR38G to J.A.H.), and the David E. King Fieldwork Award from the Department

of Geosciences at Stony Brook University. We are grateful to Scott McLennan, Chris Fedo, Troy Rasbury and Tim Glotch for fruitful discussions on the subject matter presented here. The authors would also like to thank Steven Jaret and Nicholas DiFrancesco for their assistance in the analysis of the clay fraction for elemental data. Two anonymous reviewers are acknowledged for their contributions and help in improving the manuscript.

APPENDIX A. SUPPLEMENTARY MATERIAL

Supplementary data to this article can be found online at https://doi.org/10.1016/j.gca.2019.08.003.

REFERENCES

Allen P. (2008) From landscapes into geological history. *Nature* **451**(7176), 274–276. https://doi.org/10.1038/nature06586.

Arnalds Ó. (2004) Volcanic soils of Iceland. *Catena* **56**(1–3), 3–20. https://doi.org/10.1016/j.catena.2003.10.002.

Arnalds Ó. (2008) Soils of Iceland. *Jokull* **58**, 409–421.

Arnalds Ó. (2010) Dust sources and deposition of aeolian materials in Iceland. *Icelandic Agric. Sci.* **23**, 3–21. https://doi.org/10.1016/j.aeolia.2016.01.004.

Arnalds Ó., Dagsson-Waldhauserova P. and Olafsson H. (2016) The Icelandic volcanic aeolian environment: processes and impacts – a review. *Aeolian Res.* **20**, 176–195. https://doi.org/10.1016/j.aeolia.2016.01.004.

Babechuk M. G., Widdowson M. and Kamber B. S. (2014) Quantifying chemical weathering intensity and trace element release from two contrasting basalt profiles, Deccan Traps, India. *Chem. Geol.* **363**, 56–75. https://doi.org/10.1016/j.chemgeo.2013.10.027.

Bain D. C. and Russell J. D. (1980) Swelling minerals in A basalt and its weathering products from Morvern, Scotland. 1. Interstratified montmorillonite-vermiculite-Illite. *Clay Miner.* **15**(4), 445–451. https://doi.org/10.1180/claymin.1980.015.4.11.

Berner R. A., Lasaga A. C. and Garrels R. M. (1983) The carbondate-silicate geochemical cycle and its effect on atmospheric carbon-dioxide over the past 100 millon years. *Am. J. Sci.* **283**(7), 641–683. https://doi.org/10.2475/ajs.283.7.641.

Berner R. A. (2004) The Phanerozoic Carbon Cycle: CO2 and O2. Oxford University Press.

Blatt H. and Jones R. L. (1975) Proportions of exposed igneous, metamorphic, and sedimentary-rocks. *Geol. Soc. Am. Bull.* **86** (8), 1085–1088. https://doi.org/10.1130/0016-7606(1975)86<1085:poeima>2.0.co;2.

Bluth G. J. S. and Kump L. R. (1994) Lithologic and climatologiic controls of river chemistry. *Geochim. Cosmochim. Acta* **58**(10), 2341–2359. https://doi.org/10.1016/0016-7037(94)90015-9.

Bouchez J., Gaillardet J., Lupker M., Louvat P., France-Lanord C., Maurice L. and Moquet J. (2012) Floodplains of large rivers: Weathering reactors or simple silos?. *Chem. Geol.* **332–333** 166–184. https://doi.org/10.1016/j.chemgeo.2012.09.032.

Brantley S. L. (2003) Reaction kinetics of primary rc-forming minerals under ambient conditions. *Treatise Geochem.* **5**, 605.

Brock R. W. (1943) Weathering of igneous rocks near Hong Kong. *Bull. Geol. Soc. Am.* **54**(4/6), 717–U756. https://doi.org/10.1130/GSAB-54-717.

Chesworth W., Dejou J. and Larroque P. (1981) The weathering of basalt and relative mobilities of the major elements at Belbex, France. *Geochim. Cosmochim. Acta* **45**(7), 1235–1243. https://doi.org/10.1016/0016-7037(81)90147-2.

Chou L. and Wollast R. (1985) Steady-state kinetics and dissolution mechanisms of albite. *Am. J. Sci.* **285**(10), 963–993. https://doi.org/10.2475/ajs.285.10.963.

Craig D. C. and Loughnan F. C. (1964) Chemical and mineralogical transformations accompanying the weathering of basic volcanic rocks. *Aust. J. Soil Res.* **2**(2), 218–234. https://doi.org/10.1071/SR9640218.

Cullers R. (1988) Mineralogical and chemical changes of soul and stread sediment formed by intense weathering of Danburg Granite, Georgia, USA. *Lithos* **21**(4), 301–314. https://doi.org/10.1016/0024-4937(88)90035-7.

Dessert C., Dupre B., Francois L. M., Schott J., Gaillardet J., Chakrapani G. and Bajpai S. (2001) Erosion of Deccan Traps determined by river geochemistry: impact on the global climate and the Sr-87/Sr-86 ratio of seawater. *Earth Planet. Sci. Lett.* **188** (3–4), 459–474. https://doi.org/10.1016/s0012-821x(01)00317-x.

Dessert C., Dupre B., Gaillardet J., Francois L. M. and Allegre C. J. (2003) Basalt weathering laws and the impact of basalt weathering on the global carbon cycle. *Chem. Geol.* **202**(3–4), 257–273. https://doi.org/10.1016/j.chemgeo.2002.10.001.

Eberl D. D. (2003) User's guide to RockJock—a program for determining quatitative mineralogy from powdered X-ray diffraction data. *U.S. Geological Survey, Open-File Report 03-78*, 03–78.

Eggleton R. A. (1987) Noncrystalline Fe-Si-Al- oxyhydroxides. *Clays Clay Miner.* **35**(1), 29–37. https://doi.org/10.1346/ccmn.1987.0350104.

Einarsson M. A. (1984) Climate of Iceland. *World Surv. Climatol.* **15**, 673–697.

Eiriksdottir E. S., Louvat P., Gíslason S. R., Óskarsson N. and Hardardóttir J. (2008) Temporal variation of chemical and mechanical weathering in NE Iceland: evaluation of a steady-state model of erosion. *Earth Planet. Sci. Lett.* **272**, 78–88. https://doi.org/10.1016/j.epsl.2008.04.005.

Fedo C. M., McGlynn I. O. and McSween H. Y. (2015) Grain size and hydrodynamic sorting controls on the composition of basaltic sediments: Implications for interpreting martian soils. *Earth Planet. Sci. Lett.* **423**, 67–77. https://doi.org/10.1016/j.epsl.2015.03.052.

Folk R. L. (1974) Petrology of Sedimentary Rocks. Hemphill Publishing Company, Austin, Texas.

Gaillardet J., Dupre B., Louvat P. and Allegre C. J. (1999) Global silicate weathering and CO2 consumption rates deduced from the chemistry of large rivers. *Chem. Geol.* **159**(1–4), 3–30. https://doi.org/10.1016/s0009-2541(99)00031-5.

Gíslason S. R. and Arnórsson S. (1993) Dissolution of primary basaltic minerals in natural waters- saturation state and kinetics. *Chem. Geol.* **105**(1–3), 117–135. https://doi.org/10.1016/0009-2541(93)90122-y.

Gíslason S. R., Arnórsson S. and Ármannsson H. (1996) Chemical weathering of basalt in southwest Iceland: effects of runoff, age of rocks and vegetative/glacial cover. *Am. J. Sci.* **296**(8), 837–907. https://doi.org/10.2475/ajs.296.8.837.

Gíslason S. R., Oelkers E. H. and Snorrason A. (2006) Role of river-suspended material in the global carbon cycle. *Geology* **34**, 49–52. https://doi.org/10.1130/g22045.1.

Goldich S. (1938) A study in rock-weathering. *J. Geol.* **46**(1), 17–58. https://doi.org/10.1086/624619.

Goldschmidt V. M. (1937) The principles of distribution of chemical elements in minerals and rocks. The seventh Hugo Muller Lecture, delivered before the Chemical Society on March 17th, 1937. *J. Chem. Soc.*, 655–673. https://doi.org/10.1039/jr9370000655.

Goudge T. A., Mohrig D., Cardenas B. T., Hughes C. M. and Fassett C. I. (2018) Stratigraphy and paleohydrology of delta channel deposits, Jezero crater, Mars. *Icarus* **301**, 58–75. https://doi.org/10.1016/j.icarus.2017.09.034.

Grotzinger J. P. (1989) Facies and evolution of Precambrian carbonate depositional systems: emergence of the modern

platform archetype. SEPM Special Publication, p. 44 (Controls on Carbonate PLatform and Basin Development).
Grotzinger J., Beaty D., Dromart G., Gupta S., Harris M. and Hurowitz J., et al. (2011) Mars sedimentary geology: key concepts and outstanding questions. *Astrobiology* **11**(1), 77–87. https://doi.org/10.1089/ast.2010.0571.
Gudmundsson A. (1995) Infrastructure and mechanics of volcanic systems in Iceland. *J. Volcanol. Geoth. Res.* **64**(1–2), 1–22. https://doi.org/10.1016/0377-0273(95)92782-q.
Hawley S. M., von Strandmann P., Burton K. W., Williams H. M. and Gíslason S. R. (2017) Continental weathering and terrestrial (oxyhydr)oxide export: comparing glacial and non-glacial catchments in Iceland. *Chem. Geol.* **462**, 55–66. https://doi.org/10.1016/j.chemgeo.2017.04.026.
Hemond C., Arndt N. T., Lichtenstein U., Hofmann A. W., Oskarsson N. and Steinthorsson S. (1993) The heterogeneous Iceland plume-Nd-Sr-O isotopes and trace element constraints. *J. Geophys. Res. Solid Earth* **98**(B9), 15833–15850. https://doi.org/10.1029/93jb01093.
Holdren G. R. and Speyer P. M. (1985) pH dependent changes in the rates and stoichiometry and dissolution of an alkali feldspar at room-temperature. *Am. J. Sci.* **285**(10), 994–1026. https://doi.org/10.2475/ajs.285.10.994.
Hurowitz J. A., Grotzinger J. P., Fischer W. W., McLennan S. M. and Milliken R. E., et al. (2017) Redox stratification of an ancient lake in Gale crater, Mars. *Science* **356**(6341), 922–932. https://doi.org/10.1126/science.aah6849.
Jakobsson S. P. (1972) Chemistry and distribution pattern of recent basaltic rocks in Iceland. *Lithos* **5**, 365–386. https://doi.org/10.1016/0024-4937(72)90090-4.
Jakobsson S., Jónsson J. and Shido F. (1978) Petrology of the Western-Reykjanes-Peninsula, Iceland. *J. Petrol.* **19**(4), 669–705. https://doi.org/10.1093/petrology/19.4.669.
Jakobsson S. P., Jonasson K. and Sigurdsson I. A. (2008) The three igneous rock series of Iceland. *Jokull* **58**, 117–138.
Johnasson H. and Semundsson K. (1989) Geological Map of Iceland. 1: 500000. Bed Rock Geologgy. *Icelandic Museum Natl. Hist. Icelandic Geodetic Surv.* **1**.
Johnsson M. J. (1993) The system controlling the composition of clastic sediments. In *Processes Controlling the Compsition of Clastic Sediments*, vol. 284 (eds. M. J. Johnsson and A. Basu). Geological Society of America Special Paper, Boulder, Colorado.
Jónasson K. (2007) Silic volcanism in Iceland: composition and distribution within the active volcanic zones. *J. Geodyn.* **43**, 101–117. https://doi.org/10.1016/j.jog.2006.09.004.
Kump L. R., Brantley S. L. and Arthur M. A. (2000) Chemical, weathering, atmospheric CO2, and climate. *Annu. Rev. Earth Planet. Sci.* **28**, 611–667. https://doi.org/10.1146/annurev.earth.28.1.611.
Larsen D. J., Miller G. H., Geirsdóttir Á. and Thordarson T. (2011) A 3000-year varved record of glacier activity and climate change from the proglacial lake Hvitarvatn, Iceland. *Quaternary Sci. Rev.* **30**(19–20), 2715–2731. https://doi.org/10.1016/j.quascirev.2011.05.026.
Lasaga A. C., Soler J. M., Ganor J., Burch T. E. and Nagy K. L. (1994) Chemica-weathering rate laws and global geochemical cycles. *Geochim. Cosmochim. Acta* **58**(10), 2361–2386. https://doi.org/10.1016/0016-7037(94)90016-7.
Louvat P. and Allegre C. J. (1997) Present denudation rates on the island of Reunion determined by river geochemistry: basalt weathering and mass budget between chemical and mechanical erosions. *Geochim. Cosmochim. Acta* **61**(17), 3645–3669. https://doi.org/10.1016/s0016-7037(97)00180-4.
Louvat P. and Allegre C. J. (1998) Riverine erosion rates on Sao Miguel volcanic island, Azores archipelago. *Chem. Geol.* **148**(3–4), 177–200. https://doi.org/10.1016/s0009-2541(98)00028-x.
Louvat P., Gíslason S. R. and Allegre C. J. (2008) Chemical and mechanical erosion rates in Iceland as deduced from river dissolved and solid material. *Am. J. Sci.* **308**(5), 679–726. https://doi.org/10.2475/05.2008.02.
Ma J. L., Wei G. J., Xu Y. G., Long W. G. and Sun W. D. (2007) Mobilization and re-distribution of major and trace elements during extreme weathering of basalt in Hainan Island, South China. *Geochim. Cosmochim. Acta* **71**(13), 3223–3237. https://doi.org/10.1016/j.gca.2007.03.035.
McLennan S. M. (1989) Rare earth elements in sedimentary rocks - influence of procenance and sedimentary processes. *Rev. Mineral.* **21**, 169–200.
McLennan S. M., Hemming S., McDaniel D. K. and Hanson G. N. (1993) Geochemical approaches to sedimentation, provenance, and tectonics. *Geol. Soc. Am. Spec. Pap.* **284**, 21–40.
Merriman R. J. (2005) Clay minerals and sedimentary basin history. *Eur. J. Mineral.* **17**(1), 7–20. https://doi.org/10.1127/0935-1221/2005/0017-0007.
Meunier A. (2005) Clays. Springer-Verlag Berlin Heidelberg, Germany.
Meybeck M. (1986) Composition Chimique Des Ruisseaux Non Pollues De France. *Sci. Geol Bull* **39**(1), 3–77.
Meybeck M. (1987) Global chemical-weathering of surficial rocks estimated from river dissolved loads. *Am. J. Sci.* **287**(5), 401–428. https://doi.org/10.2475/ajs.287.5.401.
Moore D. M. and Reynolds, Jr, R. C. (1997) X-ray Diffraction and the Identification and Analysis of Clay Minerals. Oxford University Press, New York.
Nahon D. B. and Colin F. (1982) Chemical weathering of orthopyroxenes under lateritic conditions. *Am. J. Sci.* **282**(8), 1232–1243. https://doi.org/10.2475/ajs.282.8.1232.
Nesbitt H. W. (2003) Petrogenesis of siliciclastic sediments and sedimentary rocks (Vol. Geo text 4). Geological Association of Canada, Canada.
Nesbitt H. W. and Wilson R. E. (1992) Recent chemical-weathering of basalts. *Am. J. Sci.* **292**(10), 740–777. https://doi.org/10.2475/ajs.292.10.740.
Nesbitt H. W. and Young G. M. (1982) Early proterozoic climates and plate motions inferred from major element chemistry of Lutities. *Nature* **299**(5885), 715–717. https://doi.org/10.1038/299715a0.
Nesbitt H. W. and Young G. M. (1984) Prediction of some weathering trends of plutonic and volcanic-rocks based on thermodynaics and kinetic considerations. *Geochim. Cosmochim. Acta* **48**(7), 1523–1534. https://doi.org/10.1016/0016-7037(84)90408-3.
Nesbitt H. W., Young G. M., McLennan S. M. and Keays R. R. (1996) Effects of chemical weathering and sorting on the petrogenesis of siliciclastic sediments, with implications for provenance studies. *J. Geol.* **104**(5), 525–542. https://doi.org/10.1086/629850.
Norrish K. and Chappell B. W. (1967) X-ray Fluorescence Spectrography. Academic Press, London.
Óskarsson B. V., Riishuus M. S. and Arnalds Ó. (2012) Climate-dependent chemical weathering of volcanic soils in Iceland. *Geoderma* **189**, 635–651.
Patino L. C., Velbel M. A., Price J. R. and Wade J. A. (2003) Trace element mobility during spheroidal weathering of basalts and andesites in Hawaii and Guatemala. *Chem. Geol.* **202**(3–4), 343–364. https://doi.org/10.1016/j.chemgeo.2003.01.002.
Potts P. J. (1992) A Handbook of Silicate Rock Analysis. Springer, New York.

Price J. R. and Velbel M. A. (2003) Chemical weathering indices applied to weathering profiles developed on heterogeneous felsic metamorphic parent rocks. *Chem. Geol.* **202**(3–4), 397–416. https://doi.org/10.1016/j.chemgeo.2002.11.001.

Raiswell R., Tranter M., Benning L. G., Siegert M., De'ath R., Huybrechts P. and Payne T. (2006) Contributions from glacially derived sediment to the global iron (oxyhydr)oxide cycle: implications for iron delivery to the oceans. *Geochim. Cosmochim. Acta* **70**, 2765–2780. https://doi.org/10.1016/j.gca.2005.12.027.

Rampe E. B., Ming D. W., Blake D. F., Bristow T. F., Chipera S. J. and Grotzinger J. P., et al. (2017) Mineralogy of an ancient lacustrine mudstone succession from the Murray formation, Gale crater, Mars. *Earth Planet. Sci. Lett.* **471**, 172–185.

Rooney A. D., Macdonald F. A., Strauss J. V., Dudas F. O., Hallmann C. and Selby D. (2014) Re-Os geochronology and coupled Os-Sr isotope constraints on the Sturtian snowball Earth. *Proc. Natl. Acad. Sci. USA* **111**(1), 51–56. https://doi.org/10.1073/pnas.1317266110.

Sæmundsson K. (1979) Outline of the geology of Iceland. *Jökull J.* **29**, 7.

Sigmarsson O., Condomines M. and Fourcade S. (1992) Mantle and curstal contribution in the genesis of recent basalts from off-rift zones in Iceland-constraints from the Th-isotopes, Sr-isotopes, and O-isotopes. *Earth Planet. Sci. Lett.* **110**(1–4), 149–162. https://doi.org/10.1016/0012-821x(92)90045-w.

Sigmarsson O. and Steinthórsson S. (2007) Origin of Icelandic basalts: a review of their petrology and geochemistry. *J. Geodyn.* **43**(1), 87–100. https://doi.org/10.1016/j.jog.2006.09.016.

Środon J., Drits V., McCarty D., Hsieh J. and Eberl D. (2001) Quantitative X-ray diffraction analysis of clay-bearing rocks from random preparations. *Clays Clay Miner.* **49**(6), 514–528. https://doi.org/10.1346/CCMN.2001.0490604.

Stumm W. and Morgan J. J. (1996) Aquatic chemistry: Chemical Equilibria and Tates in Natural Waters, 3rd ed. John Wiley & Sons Inc..

Tang M., Chen K. and Rudnick R. L. (2016) Archean upper crust transition from mafic to felsic marks the onset of plate tectonics. *Science* **351**(6271), 372–375. https://doi.org/10.1126/science.aad5513.

Taylor S. R. and McLennan S. M. (1985) The Continental Crust: its Composition and Evolution. Blackwell Scientific Publications, Oxford.

Taylor S. R. and McLennan S. M. (1995) The geochemical evolution of the continental crust. *Rev. Geophys.* **33**(2), 241–265. https://doi.org/10.1029/95rg00262.

Thordarson T. and Höskuldsson Á. (2008) Postglacial volcanism in Iceland. *Jokull* **58**, 197–228.

Wada K., Arnalds O., Kakuto Y., Wilding L. P. and Hallmark C. T. (1992) Clay minerals of 4 souls formed in eolian and tephra materials in Iceland. *Geoderma* **52**(3–4), 351–365. https://doi.org/10.1016/0016-7061(92)90046-a.

White A. F. and Blum A. E. (1995) Effects of climate on chemical weathering in watersheds. *Geochim. Cosmochim. Acta* **59**(9), 1729–1747. https://doi.org/10.1016/0016-7037(95)00078-e.

White A. F. and Brantley S. L. (1995) Chemical weathering rates of silicate minerals in soils. *Chem. Weathering Rates Silicate Miner.* **31**, 407–461.

White A. F., Blum A. E., Bullen T. D., Vivit D. V., Schulz M. and Fitzpatrick J. (1999) The effect of temperature on experimental and natural chemical weathering rates of granitoid rocks. *Geochim. Cosmochim. Acta* **63**(19–20), 3277–3291. https://doi.org/10.1016/S0016-7037(99)00250-1.

White W. M. (2013) Geochemistry John Wiley & Son, Ltd., Publication. Wiley-Blackwell.

Wilson S. A. (1998) Data Compliation for USGS Reference Material BHVO-2, Hawaiian Basalt. *U.S. Geological Survey Open-File Report xxxxx.*.

Wood D. A., Joron J. L., Treuil M., Norry M. and Tarney J. (1979) Elemental and Sr isotope variations in basic lavas from Iceland and the surrounding ocean floor. *Contrib. Miner. Petrol.* **70**, 319–339. https://doi.org/10.1007/BF00375360.

Associate editor: Jerome Gaillardet